SOLAR FUELS BY PHOTOELECTRO CATALYTIC REDUCTION OF CO_2

HPCL-NCCR-IITM

Collaborative research project

Final Report



National Centre for Catalysis Research

Indian Institute of Technology, Madras, Chennai

January-2020

SOLAR FUELS BY PHOTO ELECTROCATALYTIC REDUCTION OF CO_2

Research project sponsored by HPCL R&D to NCCR, IIT Madras

Key results from the project

- PEC cells, small and large in volume, to accommodate working electrode area- 3.12 to 12.5 cm^2 have been designed, fabricated and used for photo catalytic reduction (PECR) of CO_2 in batch mode up to 12 hrs of operation
- Synthesis and characterization of seven different semi-conductors and exploring their application as working electrode/photo anodes for PECR of CO_2
- Different electrolytes, aqueous $NaHCO_3$, $KHCO_3$ and $NaHCO_3$ + Na_2CO_3 buffer at pH-9 were explored for optimum performance. 0.5M $KHCO_3$ is the ideal choice
- Three photo anode materials, namely,
    - Au-N & Fe co-doped $Na_{(1-x)}La_xTaO_{(3+x)}$
    - Au-N, S & Fe co-doped $Sr_3Ti_2O_7$
    - Au-N, S & Fe co-doped $La_2Ti_2O_7$

  capable of photo electro catalytic reduction of CO_2 to methane at very low applied/ bias voltage of 0.1-0.5V have been developed.
- With Au-N, S & Fe co-doped $La_2Ti_2O_7$ as photo anode and Pt foil as counter electrode, 9.8 nano moles /cm^2 of methane formation from CO_2 was observed
- Strategies for improving hydrocarbon yields, like,
    - Optimization of applied voltage and increasing cell volume and electrode area,
    - Using organic bases to increase CO_2 solubility, Sensitizers to improve visible light harvesting, Counter electrodes coated with metal and alloy nano particles
    - Application of higher bias voltage,

  have been studied and optimized
- Choice of suitable photo anode, increasing the electrode area, choice of nano size metal alloy coated counter electrode and the design of electrochemical cell for continuous operation would enhance the potential of this technique for large scale applications

- CO_2 from any point source could be used for conversion to hydrocarbons /solar fuels, thus paving way for sustainable energy generation.

CONTENTS

SOLAR FUELS BY PHOTO ELECTRO CATALYTIC REDUCTION OF CO_2

1.INTRODUCTION

During the years 2010-2013, HPCL R&D & NCCR-IIT Madras were engaged in a collaborative research programme for the development of photo catalysts for the conversion of CO_2 and water into hydrocarbons (methane, methanol etc.) using simulated solar radiation. Highly efficient photo catalysts like $NaTaO_3$ and $Sr_3Ti_2O_7$ with a range of co-catalysts (Pt, Pd, Ag, Au, CuO, NiO & RuO_2) and dopants (N, S & Fe_2O_3) were identified. Five patents covering these formulations and the photo chemical conversion process have been filed. Given the low CO_2 conversion levels and low product selectivity realized with simple/direct photo catalytic conversions, it is proposed to provide additional means of activation by electro catalysis, so as to achieve higher CO_2 conversions. Besides, electro catalytic reduction of CO_2 provides means of improving selectivity to specific products. In this respect, the project on photo electro catalytic reduction (PECR) of CO_2 to solar fuels (hydrogen and hydrocarbons) is the logical extension of the earlier project on photo catalytic reduction. Development of photo anodes that absorb maximum light energy, electro catalysts that bring about oxidation- reduction reactions and the design of the photo electrochemical (PEC) cells are the key components of the project.

2.RELEVANCE OF THE PROJECT

Atmospheric CO_2 is utilized for the natural photosynthesis process, which releases oxygen, essential for the survival of all living organisms on earth, including human beings. However, abnormal increase in the emission of CO_2 since the industrial revolution, up to 400 ppm in

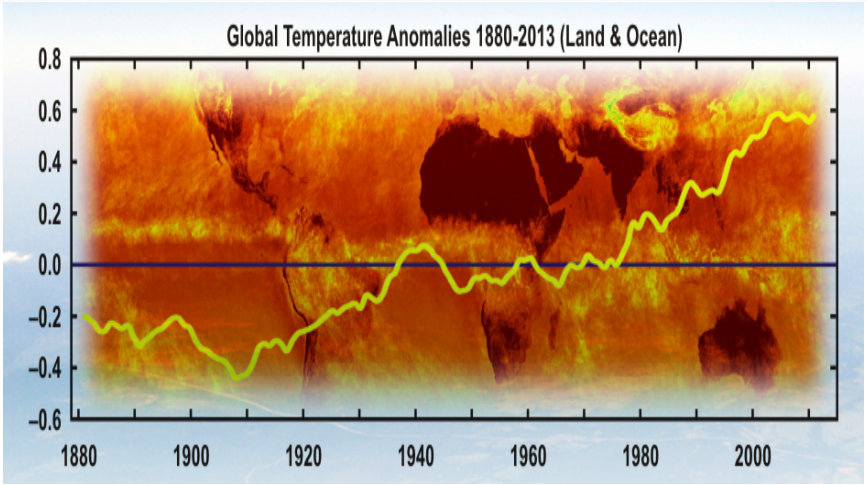

Fig.1. Global warming-Change in earth surface temperature over the years (1)

2016 (1) poses serious threat to the ecological system, wherein a fine balance in CO_2 levels between atmosphere, land and ocean is maintained. This equilibrium is disturbed by the increase in CO_2 emission, due to anthropogenic emission from the burning of fossilized matter, resulting in uneven distribution of CO_2 and consequently, global warming effect (Fig.1)

One of the key challenges in the energy front is the mitigation of green-house gas (GHG) emissions and the consequent global warming issues, which is very well reflected in drastic changes in the weather patterns observed round the world. Such a situation has led to a surge in the research efforts towards capturing and recycling of CO_2 by conversion (2) into hydrocarbon fuels and chemicals (methane, methanol etc.). Developing energy conversion processes with low carbon foot print, from sustainable energy resources, is the right strategy in this direction. Since CO_2 constitutes 90% of GHG, several processes, like chemical. thermo and radio chemical, photo chemical (PCR), photo biochemical, electrochemical (ECR) and photo electrochemical (PECR) process for conversion of CO_2 to fuels, aiming at recycling and containing atmospheric CO_2 levels, are under development (3). While PCR & ECR represent one additional mode of activation (light and electricity respectively) besides thermo catalytic activation, PECR involves simultaneous application of two additional modes (photo and electrolytic) of activation and hence expected to be more efficient. Photo electro catalysis deals with the generation of electricity by harnessing the abundant solar energy and utilize it for hydrogen production by splitting of water and reduction of carbon dioxide to hydrocarbons/solar fuels (solar fuels).

Major routes for valorization of CO_2 at various stages of development are indicated by Rhodia as shown in Fig.2 below.

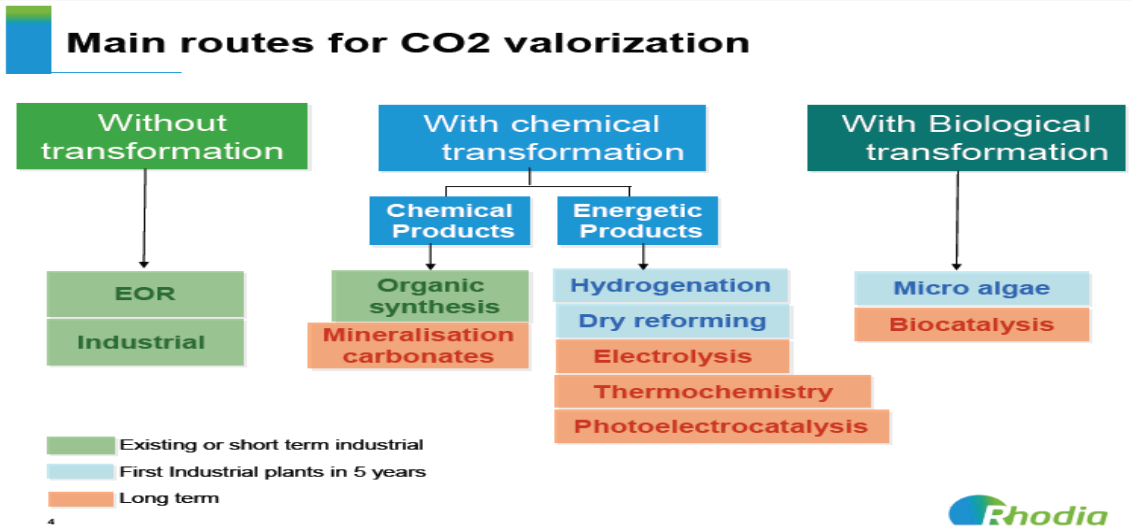

Fig.2 Major routes for valorization of CO_2 at various stages of development

The essential criterion for the preferred CO_2 conversion process is, that it has to be a sustainable one, utilizing renewable energy source, with zero carbon footprint. In this respect, the processes that are based on solar radiation, the eternal source of energy, are the ideal ones worth pursuing. Hydrogen, produced by splitting of water and hydrocarbons by reduction of CO_2 with water, using solar energy, are called as solar fuels. Considerable progress has been achieved (4) in all these processes though their practical implementation remains with a question mark.

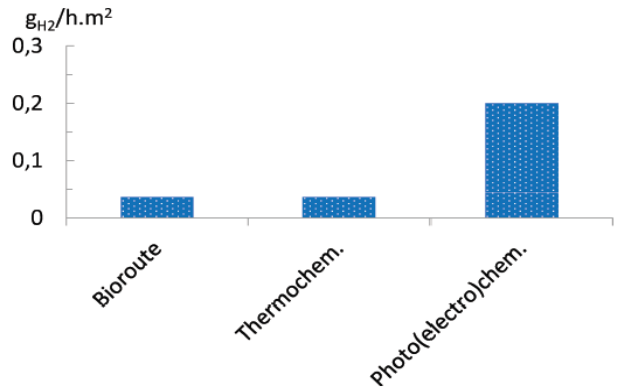

Fig.3 Comparison of the productivities of hydrogen by different routes

As indicated earlier, photochemical, electrochemical and photo electro-chemical routes could be potentially viable routes in the long term. Similarly, amongst the alternative routes for the production of H_2, the other solar fuel, maximum yields are obtained by PEC process (Fig.3). Additionally, these processes are amenable to up scaling, to enable practical applications. Hence production of H_2 and reduction of CO_2 by PEC routes are being explored with great interest. This trend has prompted NCCR to publish a Monograph on CO_2 valorization (3) that could act as a guide for the researchers, academic as well as industrial.

3.MAJOR ROUTES FOR THE CONVERSION OF CO_2 TO SOLAR FUELS

a. Photo chemical reduction (PCR) of CO_2

PCR of CO_2 with water as reductant or source of hydrogen involves utilization of photo generated electrons for simultaneous splitting of water **(**to get hydrogen) and reduction of CO_2 to hydrocarbons with sunlight as the source of energy. Developments in this field have been covered by several reviews (3-9), the recent ones being by Izumi (10) and Corma and Gracia (11).Though several catalyst systems have been found to be useful for PCR of CO_2 to hydrocarbons, CO_2conversions are extremely low, in terms of micromoles/g or around 1-2% with respect to dissolved CO_2 (12). A range of products, methanol and ethanol, besides, methane, ethane and acetaldehyde are formed. Oxidation of the hydrocarbon products by oxygen from splitting of water, reverse reaction to form water, limited solubility of CO_2 and shorter catalyst life are the major impediments in further development of the process. In spite of using co-catalysts and coupling of conduction bands to effectively separate charge carriers, recombination continues to be the major hurdle towards achieving higher conversions.

b. Electro catalytic reduction (ECR) of CO_2

The synthesis of hydrocarbons from CO_2 by ECR is a complex multistep reaction with adsorbed intermediates, most notably adsorbed CO. The exact reaction mechanisms, leading to the various products, are yet to be understood clearly and are likely to change over the range of conditions at which data has been reported. The reaction product distribution is also very sensitive the surface crystal structure copper electrode. Reaction conditions (potential, buffer strength and local pH, local CO2 concentration, stirring, and CO2 pressure influence the course of the reaction (13).

Electrochemical reactors provide three interesting advantages (14) over pure heterogeneous chemical reactors: (i) electrochemical devices are not limited by traditional thermochemical cycles, since the achievable efficiency is most often significantly higher than their chemical/combustion counterpart; (ii)direct control of the surface free energy of the catalyst through the electrode potential is possible. This allows the reaction rate and selectivity to be controlled precisely; and (iii) non-direct reaction between precursors through complementary redox processes on two separate catalysts, which permits researchers to tailor the properties needed for each redox process independently. This can facilitate different reaction pathways depending on catalyst selection with identical precursors at the same temperature, etc. while minimizing competition between alternate pathways. Depending on the process conditions several pathways are possible for the electrochemical conversion of CO_2(Fig.4)

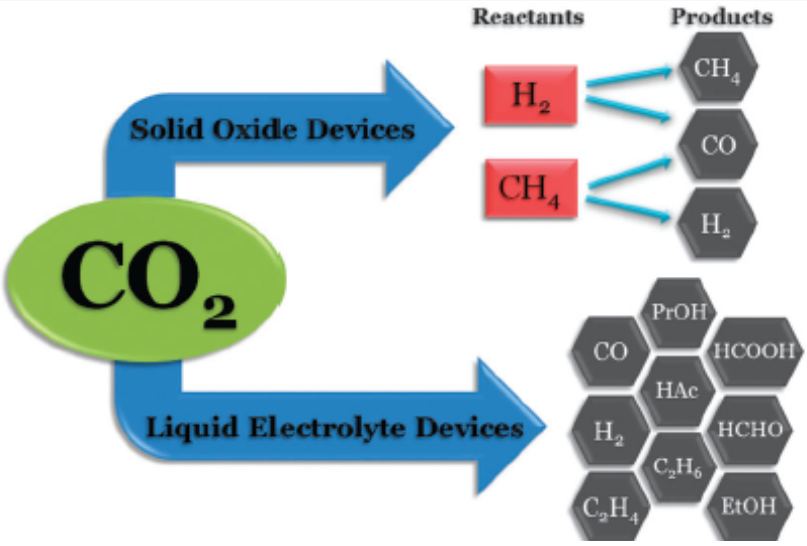

Fig.4 Reaction pathways during electrochemical reduction of CO_2(14)

Transition metals and metal oxides are commonly used for ECR of CO_2 to hydrocarbons and some general guidelines about different catalysts and the products obtained have been obtained (15).

A. Hydrocarbons and alcohols (Cu).

B. Carbon monoxide (Au, Ag, Zn, Pd, and Ga).

C. Formic acid (Pb, Hg, In, Sn, Bi, Cd, and Tl).

D. Some metals do not exhibit useful catalytic properties under typical reaction conditions, e.g.,1atm CO2 partial pressure, 25 °C (Ni, Pt, Fe, Co, Rh, Ir, and W). However, this situation can change when the conditions are modified.

E. Some metals heavily favor hydrogen evolution even if the reaction conditions are modified (Ti, Nb, Ta, Mo, Mn, and Al).

Copper based electrodes are used widely (13). Product slate depends on the structure of the electrode, nature of electrolyte and reaction conditions. Some of the disadvantages associated with the ECR of CO_2 under ambient conditions are:

- Potentials as high as 4 V are to be applied
- At this high voltage H_2 liberation becomes predominant

$2H^+ + 2e \longrightarrow H_2$; E+0.000 Vs NHE

$2H_2O + 2e \longrightarrow H_2 + 2OH^-$ E0 =- 0.828 V Vs NHE

2H+ + 2e_ - H2; E0 = 0.000 V vs. NHE

- High surface area and surface-modified copper electrodes have a high selectivity at low temperatures towards simple hydrocarbons like ethylene (C_2H_4) and CH_4, but numerous other products have also been reported, such as CO, H_2, formic acid (HCOOH), ethane, ethanol, propanol, acetic acid and lactic acid.

- Poisoning of these copper electrodes is a common issue that plagues long-term operation and limits its commercial application. Use of acidic solutions can result in activity losses due to copper dissolution as evidenced by increased blue colouring of the solution from aqueous copper species over time. On the other hand, highly alkaline solutions cause copper oxides to form on the electrode surface, which are generally considered undesirable, though C_2H_4 synthesis using copper oxide electrodes is observed (16) compared to pure a copper electrode. Graphitic carbon and organic intermediates like formate could poison electrode surface.

c. Photo electrocatalytic reduction (PECR) of CO_2

While electrocatalytic reduction requires external energy supply, photo electro catalytic reduction renders the process totally sustainable since renewable solar energy is used. In principle, the process involves a solar panel and photo voltaic unit to generate the required power for electrolysis and an electro catalyst to carryout reduction of CO_2. In practice, a monolithic photo electro-chemical unit (Fig.5) that has a photo active anode, which can perform dual function of light harvesting and acting as anode, is preferred.

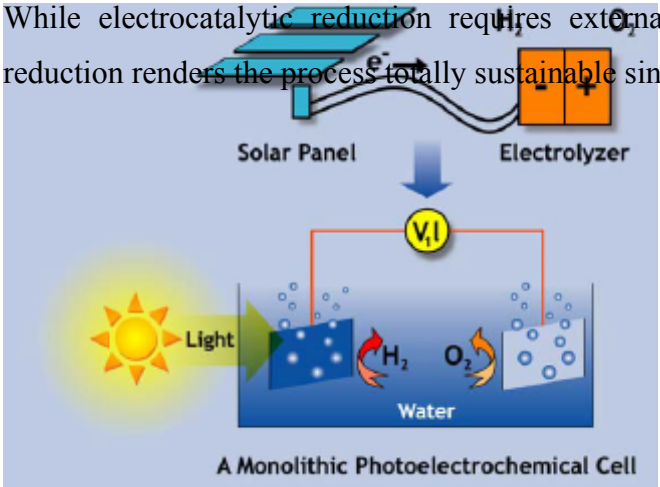

Fig.5.Conceptual PEC cell and monolithic PEC cell

Demonstration of the first PEC cell with TiO_2 as the photo anode for the production of hydrogen from water was provided by Fujishima and Honda (17)

A major advantage of PEC systems is that they involve relatively simple processes steps, and could be operated under wide operating temperature ranges, with no intrinsic upper temperature limit. The primary challenges for PEC are:

- developing materials with sufficient photovoltage to electrolyze water,
- minimization of internal resistance losses,
- developing electrodes with long lifetime (particularly corrosion life),
- maximization of photon utilization efficiencies,
- reducing plant capital cost.

The major steps in the PEC process are, light absorption, energy transfer to catalytic active sites and reactions (reduction/oxidation) at electrode/solution or electrode/gas interfaces.

The critical part of the PEC cell is the fabrication of the electrode, especially, photoactive anode.

Several designs have been evolved, the first and the simplest one being the system (Fig.6) reported by Ichikawa and Doi (18), which could be used for hydrogen generation by splitting of water and reduction of CO_2 by water. The PEC cell consists of a perforated photocatalyst (titania), a proton separator (Nafion) and a perforated electrocatalyst (platinum) into one sheet to forma SUPEC (single unit photo electro catalysis) cell as shown in Fig.6. The photocatalyst, when irradiated by light generates a pair of electron (e^-) and hole (h^+). Protons produced on the photocatalyst as a result of interaction between the hole and adsorbed water molecules ($2H_2O + 4h^+ \rightarrow 4H^+ + O_2$) can pass through the combined sheet to reach the electrocatalyst side where they can recombine electrochemically to produce hydrogen ($2H^+ + 2e^- \rightarrow H_2$. The electrons are supplied from the photocatalyst.

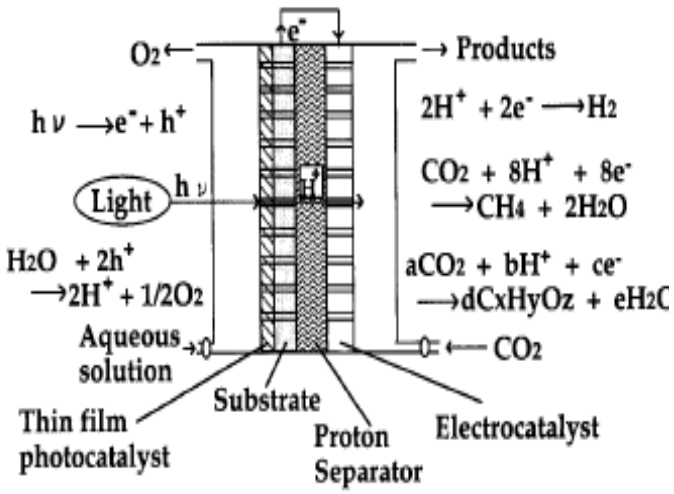

Fig.6. Single unit photo electrochemical system for water splitting and reduction of CO_2 (18)

This configuration prevents reverse reaction on the electrocatalyst (recombination of protons and oxygen to re-form the water) as the photo catalyst and the electrocatalysts do not directly touch each other. Protons are thus effectively separated and travel shortest distance to achieve high CO_2 reduction efficiency.

Quantum efficiency for production of hydrogen decreased as the crystal structure of titania was systematically varied from anatase to mixtures of anatase and rutile and then to rutile.The same trend was observed for photocurrents measured under external bias potential, thus indicating the structure sensitivity of the reaction and intrinsic advantage of anatase over futile. The anatase sample tested in a single unit photo electrocatalysis (SUPEC) cell produces hydrogen at the rates of 0.42 1/hr/ m^2 without external bias under sunlight and 26

1/hr/with bias under 500 W mercury lamp where the area is the cross section of light irradiation. Application of external bias increases the mobility of charge carriers and hence the increase in photo current generation is observed.

d. Photo electro catalysts, photo electrodes and electrolytes

A variety of materials and solutions have been studied as photo electrocatalysts and electrolytes for CO_2 reduction. Aqueous and non-aqueous solutions typically consist of a sacrificial reducing agent/electron donor along with a photo sensitizer as the photo electrocatalyst, and CO_2 is supplied as agas to the irradiated solution under an applied potential. Many commonly-used catalysts are bimetallic, n- or p-type electrodes, some of which are additionally doped. Bockris and Wass produced CO with methanol and H_2 by-products using phosphorus-doped p-type CdTe, boron-doped p-type Si, and deposited crown ether photo electrocatalysts in both aqueous and non-aqueous media (19). Use of non-aqueous solvents like methyl formamide with tetra alkyl salts resulted in high current densities (19).Solvents affect the products pattern, methanol or HCOOH as the main products using aqueous media, and CO, HCOOH, and H_2 using cold methanol electrolytes, over various bimetallic photo electrocatalysts including n-type and p-type GaAs, p-type InP, and Zn-doped p-type GaP and p-type GaAs.(20-22)

Other types of materials are complexes containing2,2'-bipyridine (bipy) with transition metals. These photosensitizers work in conjunction with other species in solution to help carry out the reduction of CO_2 under irradiation. One such complex that has been studied in both aqueous -aqueous electrolytes is $Ru(bipy)_3^{2+}$ (23-25). In acidic aqueous media, triethanolamine was added as a sacrificial electron donor and methyl viologen was used as a restorable electron relay to synthesize HCOOH. With these aqueous solutions, water acts as a plentiful hydrogen source. In non-aqueous solutions, since there is not necessarily an available source of hydrogen, small concentrations of water can be added to facilitate the synthesis of products other than just CO. Using an acetonitrile electrolyte over $Ru(bipy)_3^{2+}$ with CoCl2 as the reducing intermediate, Lehn and Ziessel varied the amount of H_2O added to the electrolyte to create syngas with controllable CO/H2 ratios (24).In another report, using a similar setup with the addition of1,10-phenanthroline–ruthenium(II) to the $Ru(bipy)_3^{2+}$ photo sensitizer, water content was altered to produce formate ions.(25).

e. Recent developments in PEC process

Design of photo active anodes, electro catalysts and PEC cell design have undergone substantial changes/advancements. Fe_2O_3nano tubes vertically aligned and decorated with CuO flower crystals were found to be good electro catalysts for the reduction of CO_2 to

methanol and ethanol (26). A simple H type PEC cell (27), with three electrodes, copper, SCE and photoactive anode of N-doped nano size TiO_2 film deposited on a conduction support and suitable electrolytes in both cathodic and anodic chambers have been used (Fig.7).

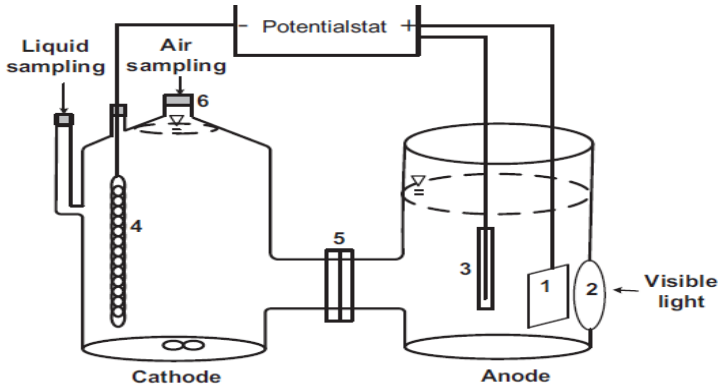

Fig.7 Schematic diagram of photoelectrochemical system: (1) photoanode (NdopedTiO$_2$ thin film) (2) quartz window (3) reference electrode (SCE) (4) counterelectrode (copper wire), (5) cation exchange membrane and (6) septum (27).

Since PEC cells with liquid electrolytes have inherent problems like low solubility of CO_2 and difficulty in the separation of products from the electrolytes, gas phase solventless PEC systems based on nano carbon and CNT have been developed by Centi and co-workers (28-33). In order to enhance the efficiency of reactions at the electrode-CO_2 gas at the interphase, Gas diffusion electrodes with gas diffusion membrane (GDM) are used.

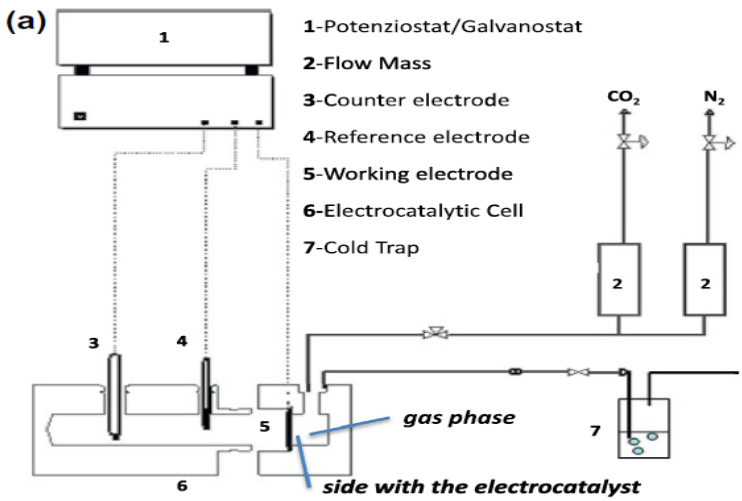

Fig.8(a) Schematic drawing of the apparatus for flow electrocatalytic tests of CO_2 conversion using solventless flow cell with electro catalyst in contact with a gaseous flux of CO_2 (28).

The essential features of such gas phase reactor are given in Fig.8a & 8 b. It has been reported that the gas phase cells with Pt nano particles on carbon based electrodes are capable of electro catalytic reduction of CO_2 to long chain hydrocarbons (29). Electro catalysts, Pt, Fe, Co & Cu nano particles based on CNT, are observed to be effective in the reduction of CO_2 to hydrocarbons (28). Attempts are being made to have a rational design of electro catalysts (34) that could be useful for H_2 production and PECR of CO_2 as well. High yields of

methanol, 1166.77 micro moles per litre after 5 hrs has been observed on Cd-Te-Se nano sheets decorated on TiO_2 nano tubes (35).

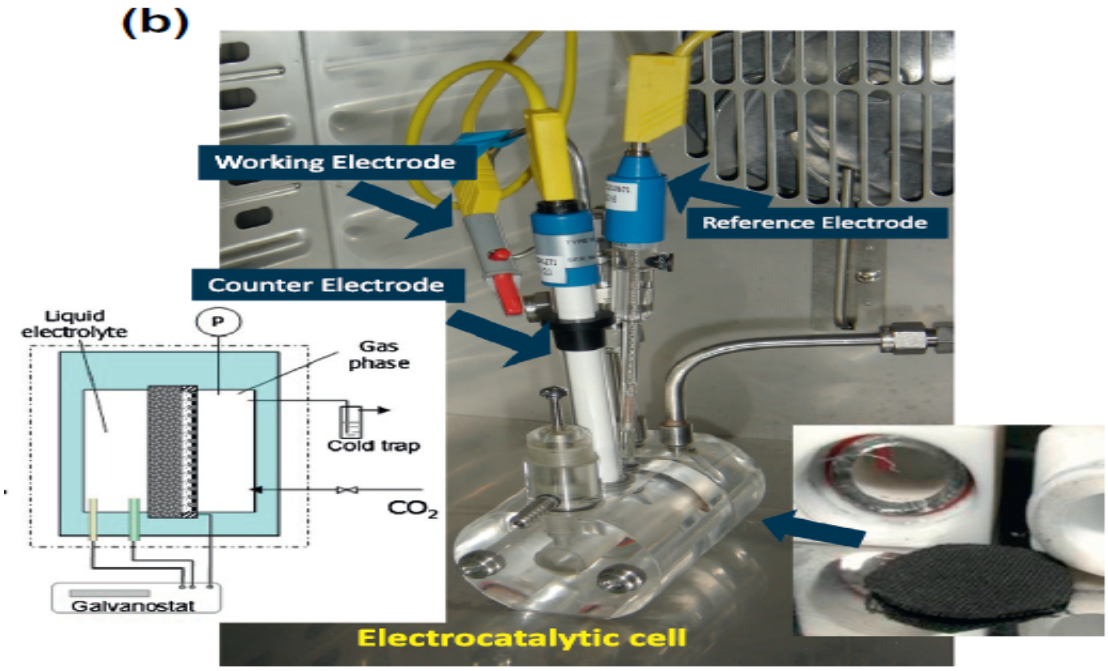

Fig.8b Photo of the cell; in the inset view of the electrode and GDM (28)

4. TYPES OF CELLS FOR PHOTO ELECTRO CATALYTIC REDUCTION OF CO_2

In a photo electro catalytic set-up, a semiconductor absorbs light energy to promote the reduction/oxidation reactions on the surfaces of electrodes. Fig.9 shows schematic

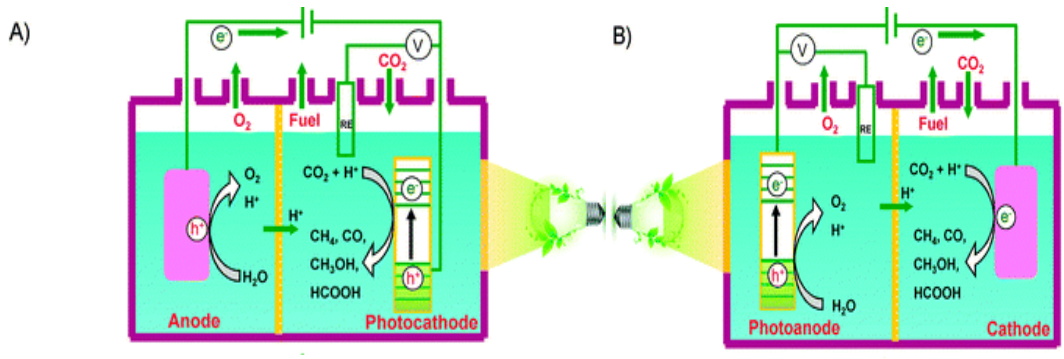

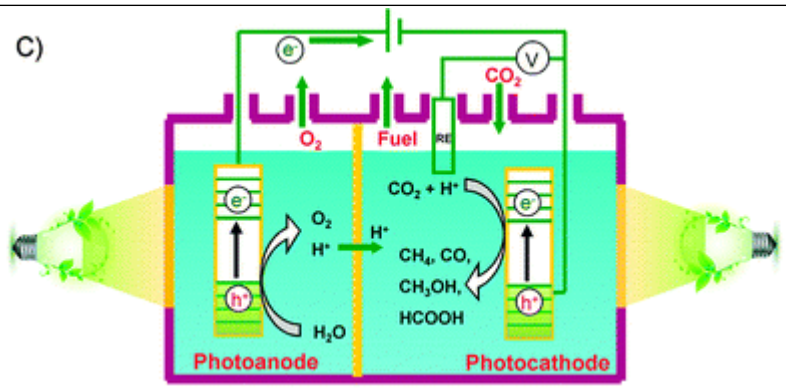

Fig.9 Schematic Representation of three possible two-compartment photo electro catalytic cells separated by proton-exchange membranes for the reduction of CO2. A. Semiconductors as photo cathodes. B. Semiconductors as photo anodes. C Semiconductors as both photo cathodes and photo anodes.

representation of three typical two compartment photo electro catalytic cells separated by proton exchange membranes. Semiconductors may be used as either photo cathodes (Fig. 9A) or photo anodes (Fig.9.B). Both electrodes can also be employed as semiconductor photo catalysts (Fig. 9.C). Both the electrodes absorb light to generate electrons and holes [36]. The holes generated at the photo anode (typically an n-type semiconductor) may oxidize H_2O to O_2 while the photo generated electrons at the photocathode (typically a p-type semiconductor) may work for the reduction of CO_2 to CO, HCOOH, methanol or hydrocarbons in the presence or absence of a co-catalyst.

5. COMPARISON OF PHOTO, ELECTRO AND PHOTO ELECTRO CATALYTIC REDUCTION OF CO_2

Typically, photo catalytic reduction of $CO_2$with water is carried out in the presence of heterogeneous semiconductor powder suspended in water. In such a case, reduction of CO_2 and oxidation of H_2O take place in the same medium/ surface of semiconductor material. After certain time, respective reverse reactions could take place, thus seriously affecting the formation of reduction products. In photo electro catalytic reduction of CO_2 (PECR) both the oxidation and reduction reactions take places in separate cells/electrodes, thus reverse reaction is avoided [37].

In the case of electro catalytic reduction, large amount of electricity must be supplied to overcome the high over potential for CO_2 reduction, which is reduced when photo electro catalytic method is adopted. PECR is the combination of photo catalysis with electro catalysis

and typically exploits semiconductor electrodes instead of normal conducting electrodes used in electro catalysis Photo electro catalytic reduction of CO_2 would reduce electricity consumption as compared to the electro catalytic reduction of CO_2 because of the introduction of solar energy. On the other hand, as compared to photo catalysis, photo electro catalysis may achieve higher efficiency because the applied external bias voltage can drive the separation of photo generated electrons and holes, which is the most crucial step in improving the photo catalytic efficiency. Besides, by applying specific bias voltage, formation of desired reduction product could be obtained, thus improving product selectivity. In typical photo catalytic reduction, a range of reduction products are formed. Features and applications of PECR have been reviewed extensively (36-39).

6.OBJECTIVES OF THE PROJECT

The objectives of the project are to:

- develop efficient electro catalysts for the conversion of CO_2 into hydrocarbons
- achieve the activation of the electro catalyst using simulated solar radiation
- design and demonstrate the functioning of photo electro catalytic (PEC) cell for the reduction of CO_2, integrating all the essential components

The project involves the development of suitable photo anodes as working electrodes (WE) stable and efficient electro catalysts as compensating electrodes/cathodes (CE) and fabrication of compact PEC cells, for the reduction of CO_2 to hydrocarbons, in batch/continuous flow modes. Efficiency of several types of working electrodes (WE) for suitable PECR of CO_2 using Pt foil as the counter electrode (CE) would be explored. Another objective is to design and explore the use of different counter electrodes to improve the conversion of CO_2 to hydrocarbons since the nature of counter electrode could also affect the efficiency and the product selectivity in CO_2 reduction.

The other objective is to study the efficiency of semiconductors that are active in the visible region. Accordingly, the following semiconductors with wide band gap have been suitably modified (by doping and sensitization) to reduce the band gap energy and enable visible light absorption and used as working electrode materials.

The following semi-conductor materials were used for the preparation of the working electrodes

1. Barium tantalate- $Ba_5Ta_4O_{15}$ co-doped with N & Fe
2. N, S & Fe co-doped meso porous titania
3. Au-N & Fe co-doped $Na_{(1-x)}La_xTaO_{(3+x)}$

4. Au-N, S & Fe co-doped $Sr_3Ti_2O_7$
5. Au-N, S & Fe co-doped $La_2Ti_2O_7$
6. $Sr_3Ti_2O_7$ sensitized with Cu phthalocyanine
7. CuO- $Sr_3Ti_2O_7$

7. EXPERIMENTAL METHODOLOGY

7.1 Chemicals used

Titanium tetrakis (butoxide), Copper (II) nitrate hexa hydrate, Iron (III) oxide, Gold (III) chloride hydrate and Sepiolite clay were obtained from Sigma Aldrich. Tantalum (V) oxide was purchased from Alfa Aesar and Strontium nitrate anhydrous from SD fine chemicals. Lanthanum oxide was procured from Loba Chemicals. Urea and Thiourea were purchased from Merck. 1.2 dicyano benzene, $CuCl_2$ and methanol were purchased from Sigma Aldrich and used as such without further purification. All other chemicals used in the investigation were of analytical (AR) grade and were obtained from Sisco Research Laboratories Pvt. Ltd. or S.D. Fine Chemicals, India.

7.2 Preparation of catalysts

7.2.1 Preparation of $Ba_5Ta_4O_{15}$

$Ba_5Ta_4O_{15}$ was prepared by simple hydrothermal method as illustrated in Scheme.1[40]. In a typical synthesis, 1.576 g $Ba(OH)_2 \cdot 8H_2O$ was dissolved in water (60 mL), to which 0.884 g of Ta_2O_5 powder was added under stirring. The resultant mixture was transferred into a 100 ml Teflon-lined stainless-steel autoclave. After hydrothermal treatment at 270 °C for 24 h, it was allowed to cool to room temperature. The white product was collected by centrifugation, washed with deionized water three times, and finally dried at 60 °C under vacuum.

The same procedure was adopted for doping of N and Fe separately and for co-doping N & Fe. Fe_2O_3 and urea were added as precursors for iron and nitrogen respectively.

7.2.2 Preparation of Fe N, S doped meso porous titanium dioxide

Meso-porous titanium dioxide was prepared by hydrothermal method as described in Scheme.2 [41]. In a typical synthesis, titanium glycolate formed in the first step was subjected to by hydrothermal treatment. Titanium glycolate precursor was synthesized by the addition of 4.26 mL Titanium tetrakis (butoxide) into a 14 mL of ethylene glycol lkept in a

100 mL flask with continuous stirring, under inert atmosphere by bubbling nitrogen for about 30 min. to remove moisture from the reaction mixture. Then the flask was sealed and kept stirring for 12 h at room temperature. The resulting mixture was poured into a 200 mL of acetone (2% water in acetone solution) and stirred for an hour. The obtained white precipitate was centrifuged

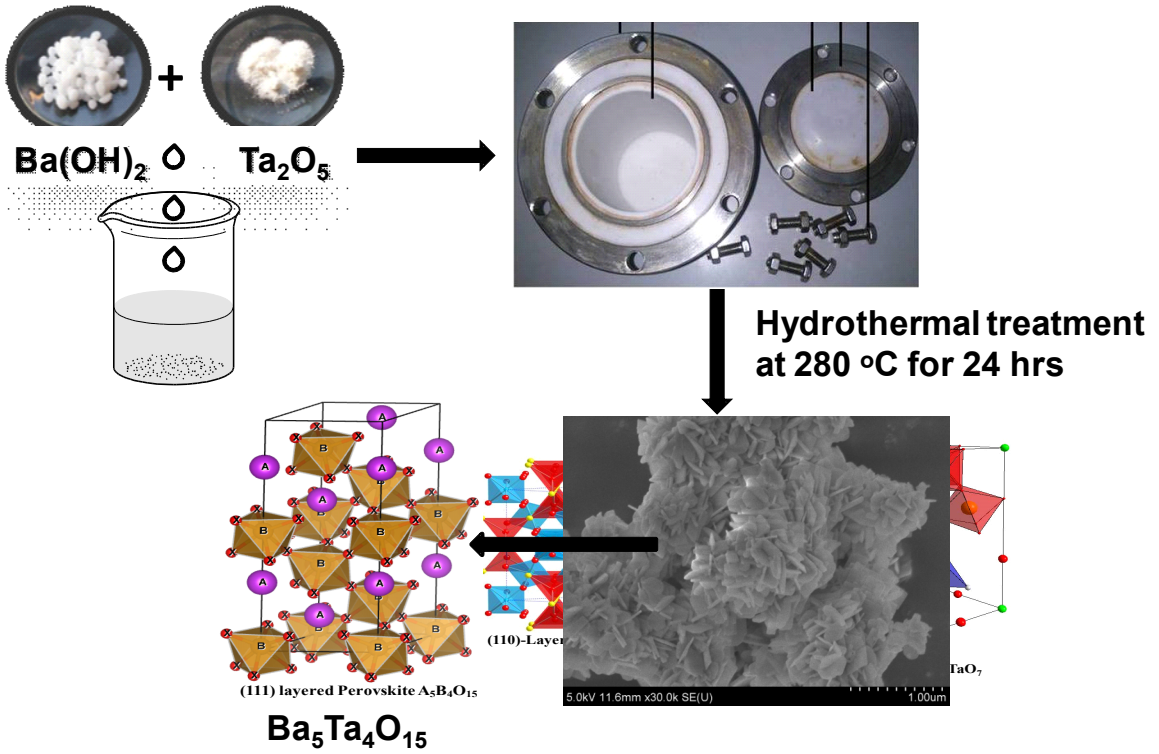

Scheme 1 Flowchart representation for the synthesis of $Ba_5Ta_4O_{15}$

and washed with ethanol. The resulting white sample was dried at 50 ºC to get titanium glycolate powder.

$$Ti(OBu)_4 + 2HOCH_2CH_2OH \longrightarrow Ti(OCH_2CH_2O)_2 + 4HOBu$$

1g of titanium glycolate powder, thio-urea (2 moles) as precursors for N-S co-doping and iron(III) oxide as Fe precursor were dispersed in 80 mL of water under ultrasonication. The resulting mixture was transferred into a teflon lined autoclave and kept in an oven at 180 °C for 4h. The resulting product was washed with water followed by ethanol and dried at 60 °C. The obtained Fe-N, S doped mesoporous titanium dioxide was denoted as FNST in subsequent discussions.

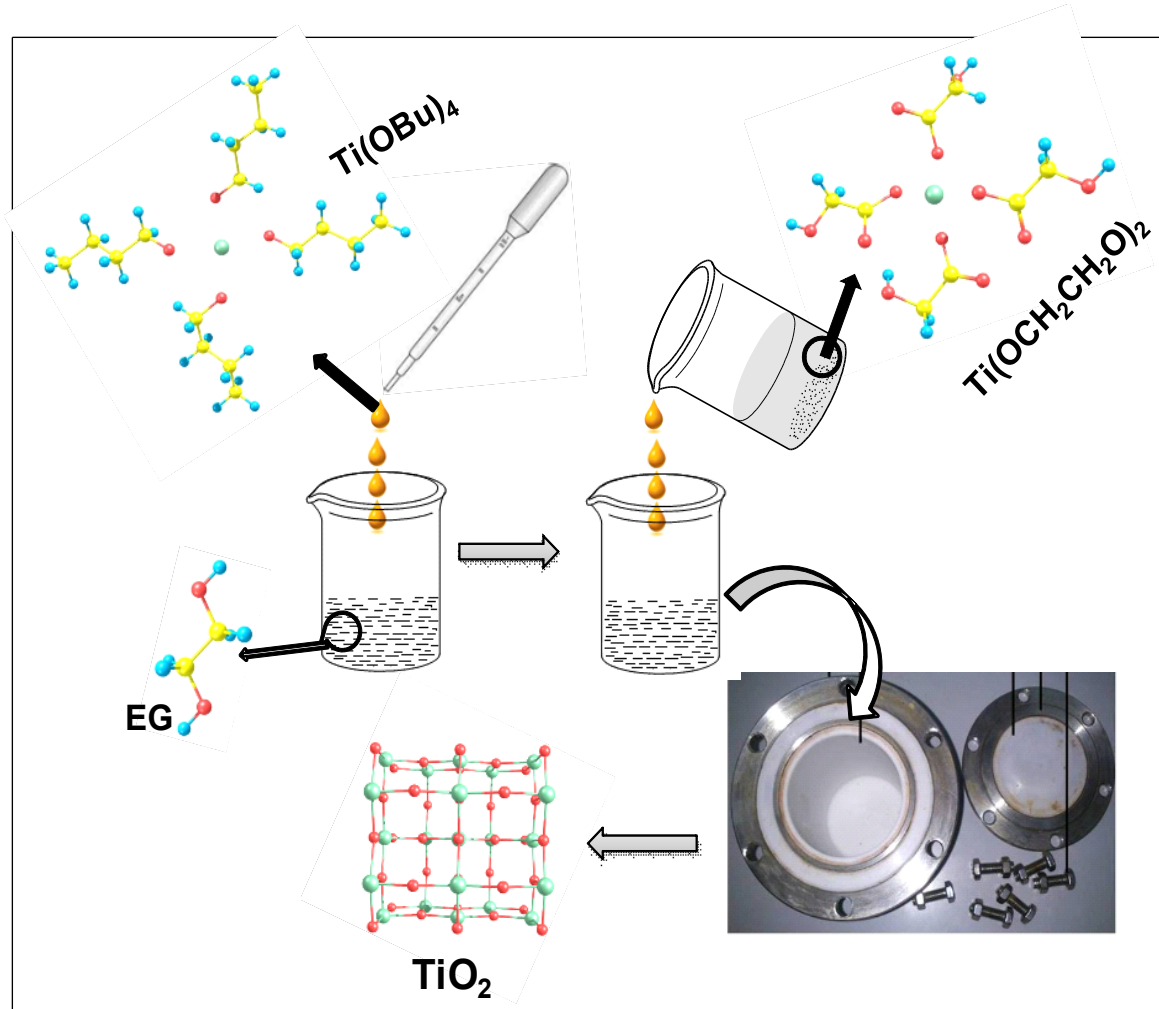

Scheme. 2 Flowchart representation for the synthesis of meso-porous titanium dioxide

7.2.3 Preparation of Fe-N modified $Na_{(1-x)}La_xTaO_{(3+x)}$

$NaTaO_3$ and 2.0% (w/w) lanthanum promoted catalysts were prepared by hydrothermal route as illustrated in Scheme3 [42]. To prepare $NaTaO_3$, 0.6 g of NaOH dissolved in 20 mL of water (0.75M) and 0.442 g of Ta_2O_5 were added into a teflon lined stainless steel autoclave. After hydrothermal treatment at 140°C for 12 h, the precipitate was collected, washed with deionized water and ethanol, finally several times with water and dried at 80 °C for 5 h.

La modified $NaTaO_3$ ($Na_{(1-x)}La_xTaO_{(3+x)}$ with x= 0.00014 for 2.0% w/w of La) was prepared by the same procedure, by adding 0.0117 g of La_2O_3 along with NaOH and Ta_2O_5 in the autoclave.

The same procedure was adopted for doping of N and Fe separately and for co-doping N & Fe. Fe_2O_3 and urea were added as precursors for iron and nitrogen respectively.

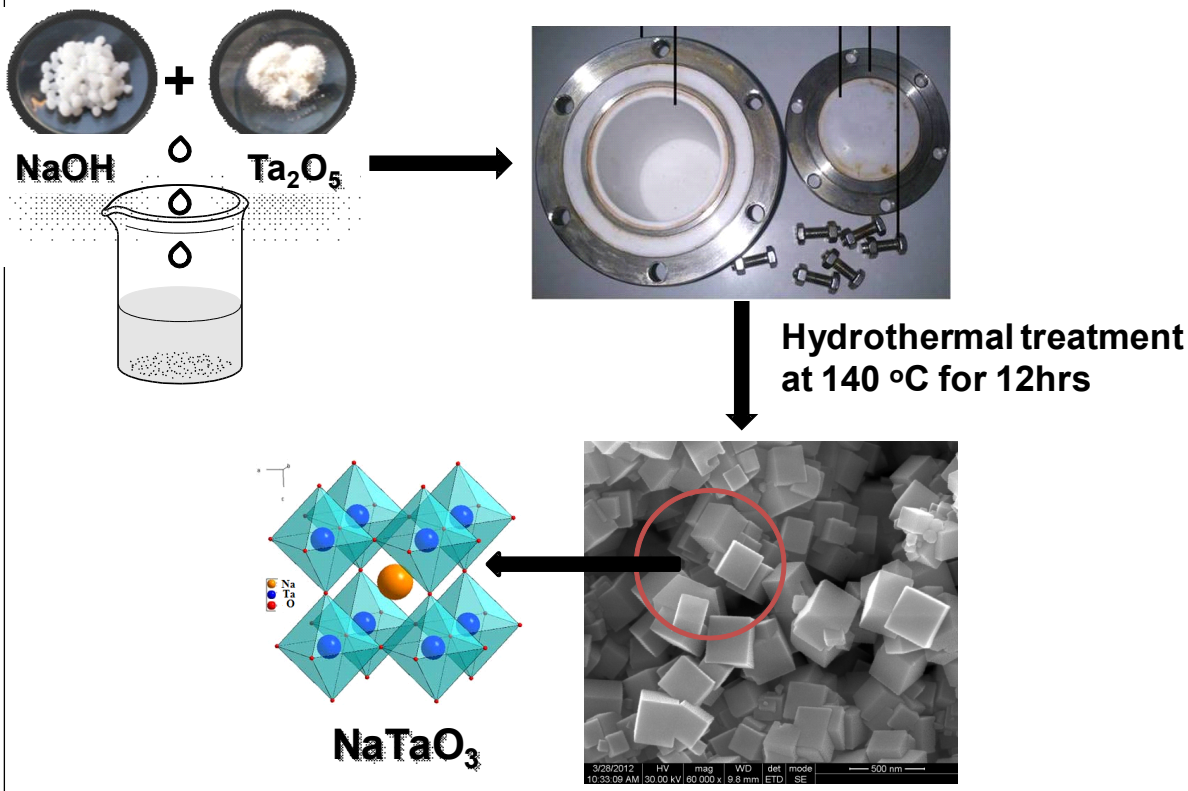

Scheme.3. Flowchart representation for the synthesis of $NaTaO_3$

7.2.4 Preparation of $Sr_3Ti_2O_7$ and doping with N, S & Fe

Neat $Sr_3Ti_2O_7$ was prepared by adopting polymer complex method, (Pechini's method) reported by Yoshino et al [43] after some modifications at our end (Scheme .4). Ethylene glycol and methanol ratio and pH of the medium were further optimized to get phase pure $Sr_3Ti_2O_7$.

Titanium tetra butoxide (2 moles) was added to a mixture of ethylene glycol and methanol (1:2 mole ratio) with vigorous stirring. To this mixture, citric acid (to get 1:0.5 mole ratio of ethylene glycol : citric acid) and strontium nitrate (3 moles as per the stoichiometry) were added. Heating the mixture at 130 °C for 20 h resulted in a polymer complex gel, which was pyrolized in air at 350 °C, followed by calcination at 900 °C for 2 hrs. Urea or thio-urea (2 moles in each case) as precursors for N doping and N-S co-doping and Fe_2O_3 powder (3wt% of Fe with respect to $Sr_3Ti_2O_7$) as such, were introduced along with strontium nitrate, prior to polyester formation to obtain doped $Sr_3Ti_2O_7$. Doped catalysts are represented by the general formulae-$Sr_3Ti_2O_7$ (neat), $Sr_3Ti_2O_{(7-x)}N_x$, $Sr_3Ti_{(2-x)}S_xO_{(7-y)}N_y$, $Sr_3Ti_{(2-x)}Fe_xO_7$, $Sr_3Ti_{(2-x)}Fe_xO_{(7-y)}N_y$, $Sr_3Ti_{(2-x-y)}Fe_xS_yO_{(7-z)}N_z$ signifying different dopant compositions

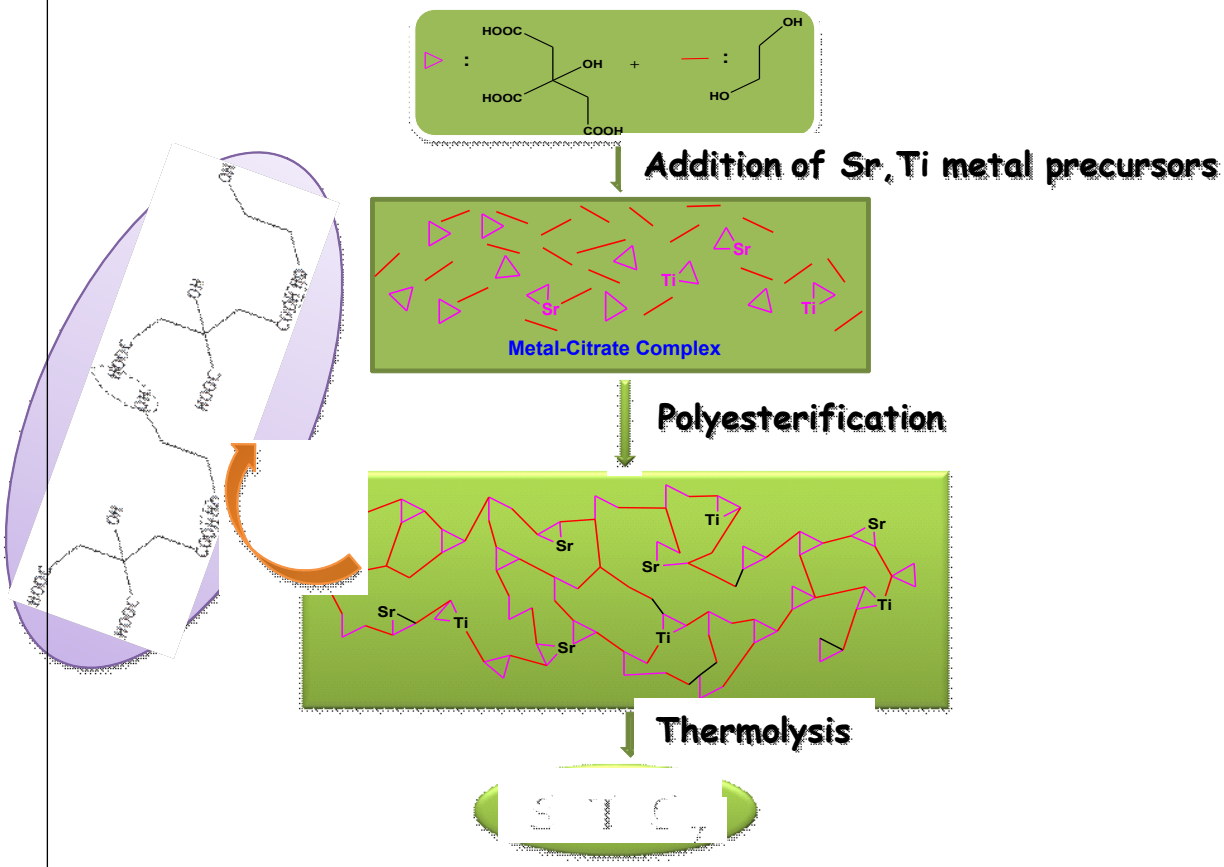

Scheme.4. Synthesis of $Sr_3Ti_2O_7$ by Polymerized Complex Method.

7.2.5 Synthesis of Copper Phthalocyanine (CuPc)

Copper Phthalocyanine (CuPc) was synthesized by adopting other metal phthalocyanine synthesis method with some modifications at our end [44]. To prepare CuPc, 4 mmol of 1,2 dicyano benzene (5.13 g) mixed with 1 mmol (1.35 g) of copper chloride and reaction mixture was slowly heated upto 140 °C under reflux. At this condition 1,4 dicyano benzene melts and forms blownish slurry with $CuCl_2$. Again the reaction vessel was heated upto 180 °C in oil bath and maintained for 2 hrs with continuous stirring. The resulting product was cooled to room temperature; grounded powder was washed with methanol, hot alcohol and water to remove unreacted components and intermediates, finally dried at 80 °C for 1 hr. The bluish copper phthalocyanine powder was recovered.

7.2.6 Preparation of CuPc sensitized $Sr_3Ti_2O_7$

1.0 w/w%-CuPc/ $Na_{(1-x)}La_xTaO_{(3+x)}$ composite was prepared by adopting previous report [45]. Briefly, 10 mg of CuPc was dissolved in 1 mL of dimethyl formamide(DMF), followed by aqueous suspension (0.99 gm in 100ml water) of $Sr_3Ti_{(2-x-y)}Fe_xS_yO_{(7-z)}N_z$support and continued stirring for 24hr. The resulting colloidal solution was filtered and obtained blue precipitate was washed with distilled water and dried in vaccum at 80 °C for 6 h. The resultant Blue colored nano composite was denoted as CuPc/STO.

7.2.7 Preparation of CuO-$Sr_3Ti_2O_7$

CuO supported on $Sr_3Ti_2O_7$were prepared by wet impregnation method. Briefly, the $Sr_3Ti_2O_7$ sample was dispersed in aqueous solution of Copper(II) nitrate hexa hydrate (for 3 wt% CuO), dried at 100°C followed by calcination in air at 300 ºC for 3 h and denoted as CuO/ $Sr_3Ti_2O_7$.

7.3 Preparation of Electrodes

Working Electrodes (WE) were prepared by applying the electro catalysts as thin coating on ITO (indium tin oxide) plates. Coated area of 1 cm^2 on ITO plate was used for CV & LSV measurements. Copper wire was glued to ITO plate to establish electrical contact. At the contact point conducting silver paint was used as the glue, which was subsequently covered with epoxy coating, to prevent contact with the electrolyte solution.

7.3.1 Preparation of semi-conductor Coating mix

90% of prepared semi-conductor +10% of Poly vinyl di-fluoride (PVDF) as binder were dissolved in the solvent, N-methyl pyrrolidone (NMP) and stirred for 30 Min to prepare the coating mix. The prepared mix was coated on ITO plate by doctor blade method

By using the above method all Electrodes are prepared by coating the different prepared (as mention in the 3.2 section) material on the ITO Plate

7.3.2 Selection of Photo electrodes

n-type semi-conductors are used as photo anodes, while p-type semiconductors as photo cathodes. Ideally, n-type semi-conductors are preferred over p-type, since they are stable in presence of electrolytes, without undergoing photo corrosion like n-type. Besides the configuration as shown in Fig.2, with n-type semi-conductors as photo anodes, enables exploring several photo anodes and designing different compensating electrodes/cathode materials so as to maximize the efficiency of the cell

7.4 Characterization of catalysts

7.4.1 X- Ray Diffraction

The crystal phase of the catalysts was analysed by X-ray diffractometer (Rigaku-MiniFlex-II) using Cu Kα radiation (λ=1.54056 Å) in the scan range of 2θ = 5-90° at a speed of 3°/min.

The crystallite sizes were calculated by the Scherrer's formula, $t = K\lambda/\beta Cos\theta$, where t is the crystallite size, K is the constant dependent on crystallite shape (0.9 for this case) and λ = 1.54056 Å, β is the FWHM (full width at half maximum) and θ is the Bragg's angle.

The phase composition of TiO_2 was analyzed using the relative peak intensity of anatase and rutile and using the formula, $FA = 1/ [1+1.26(I_R/I_A)]$, where IR – Intensity of Rutile peak, IA – Intensity of Anatase peak.

Lattice parameters for the catalyst having tetragonal crystal systemwere calculated using the formula

$1/d^2 = [h^2+k^2]/a^2 + l^2/c^2$,

Lattice parameters for the catalyst having orthorhombic crystal system was calculated using the formula

$1/d^2 = h^2 / a^2 + k^2 / b^2 + l^2 / c^2$

where h, k, l are miller indices, d is the inter planar distance and a, b, c are lattice parameters.

7.4.2 DRS UV- Visible Spectroscopy

Diffuse reflectance absorption spectra of the catalysts in the UV-Visible region were recorded using a Thermo Scientific Evolution 600 spectrophotometer equipped with a Praying Mantis diffuse reflectance accessory.

7.4.3 Photo luminescence Spectroscopy

Photoluminescence spectra were recorded under the excitation with a 450W Xenon Lamp and the spectra were collected using JobinYvon Fluorolog-3-11 spectro fluorimeter.

7.4.4 Scanning Electron Microscopy

Scanning electron micrographs were recorded using FEI, Quanta 200, equipped with EDXA attachment for elemental analysis. The samples in the powder form were taken on the carbon tape and mounted on the SEM sample holder.

7.5 Electrochemical measurements

7.5.1 Cyclic Voltammetry

Cyclic voltammetry (CV), one of the more commonly used electro analytical techniques, is an excellent method development tool, but is not usually a good technique for quantitative analysis. Its main advantage in electro analysis is its ability to characterize an electrochemical system. By using CV number of electrochemical analysis can be done some of them are given below

- The determination of Nernstian (reversible) or non-Nernstian (irreversible) behaviour of a redox couple
- The number of electrons transferred in an oxidation or reduction
- Formal potentials
- Rate constants
- Formation constants
- Reaction mechanisms
- Diffusion coefficients

In a CV experiment, the potentiostat applies a potential ramp to the working electrode to gradually change potential and then reverses the scan, returning to the initial potential

7.5.2 Liner sweep voltammetry

In linear sweep voltammetry (LSV), the electrode potential is varied at a constant rate throughout the scan and the resulting current is measured [46].

7.5.3 Controlled potential electrolysis

The principle behind the Controlled Potential Electrolysis (CPE) experiment is very simple. If only the oxidized species is initially present, then the potential is set at a constant value sufficiently negative to cause rapid reduction and is maintained at this value until only the reduced species is present in solution. The total charge passed during the CPE is calculated by multiplying the current into time.

7.6 Gas chromatography

Gas and liquid phase samples were taken out at periodic intervals with gas-tight/liquid syringes and analysed by GC. Liquid phase products (hydrocarbons) were analysed on PoroPlot Q capillary column with FID and gas phase products on Molecular Sieve 13X column with TCD.

The products were analysed using Clarus 580 Perkin Elmer Gas chromatography -

Using Poroplot Q, 30 m and the detector is FID.

Injector Temperature: 250 °C

Column Temperature: 150 °C isothermal, Hold – 20 min

Detector Temperature: 250 °C

Carrier Gas: Nitrogen, 1.5 mL/min.

All the standard gas such as Methane (10 % in N_2), ethylene, ethane, propylene and liquid standards such as formaldehyde, formic acid, methanol, acetone, acetaldehyde, ethanol were injected and their retention time were noted. Some of the liquid compounds were detected in gas phase, hence all the liquid compound were taken, purged with N_2 and then the gas phase which now contains both the compound and N_2 were injected into the GC for calibration.

Gaseous products other than hydrocarbon such as H_2 and O_2 have been analysed by TCD detector with molecular sieve 13X column

Injector Temperature: 150 °C

Column Temperature: 50 °C isothermal for 8 min.

Detector Temperature: 110 °C

Carrier gas: Nitrogen, 30 mL/min.

7.7 Photo electro catalytic reduction of carbon dioxide

All photo electro catalytic experiments were carried out in H type cell with three electrodes, working electrode (WE), reference electrode (RE) and counter electrode (CE) (Fig 10). Different types of WE are prepared by coating ITO plates with different semi-conductor materials. In the present case, WE acted as the photo anode that absorbs light energy, resulting in the generation of photo electrons and holes. A bias potential with respect to the RE is applied to WE so that the photo generated electrons travel to the CE which acts as cathode, to bring out the reduction of CO_2. 0.1 m $NaHCO_3$ or $NaHCO_3$ + Na_2CO_3 buffer at pH -9 is used as the electrolyte.

Initially, CV & LSV measurements at different applied voltage are carried out in dark after purging the electrolyte with nitrogen, followed by purging the electrolyte in the cathode compartment with CO_2 in dark for 30 min .Then the photo anode is irradiated with light from 300W Xenon lamp, fitted with AM 1.5 filter to get UV-visible light thus simulating sunlight. CV and LSV measurements are then carried out in the desired voltage range and voltage sweep rate.

CPE measurements are carried out at fixed voltage, as indicated by CV & LSV, for a specific period, 6-8 hrs with continuous irradiation of photo anode. At regular intervals liquid samples are drawn from the cathode compartment and injected into the GC for the analysis of CO_2 reduction products.

Setup for Photo electrochemical reduction of CO_2

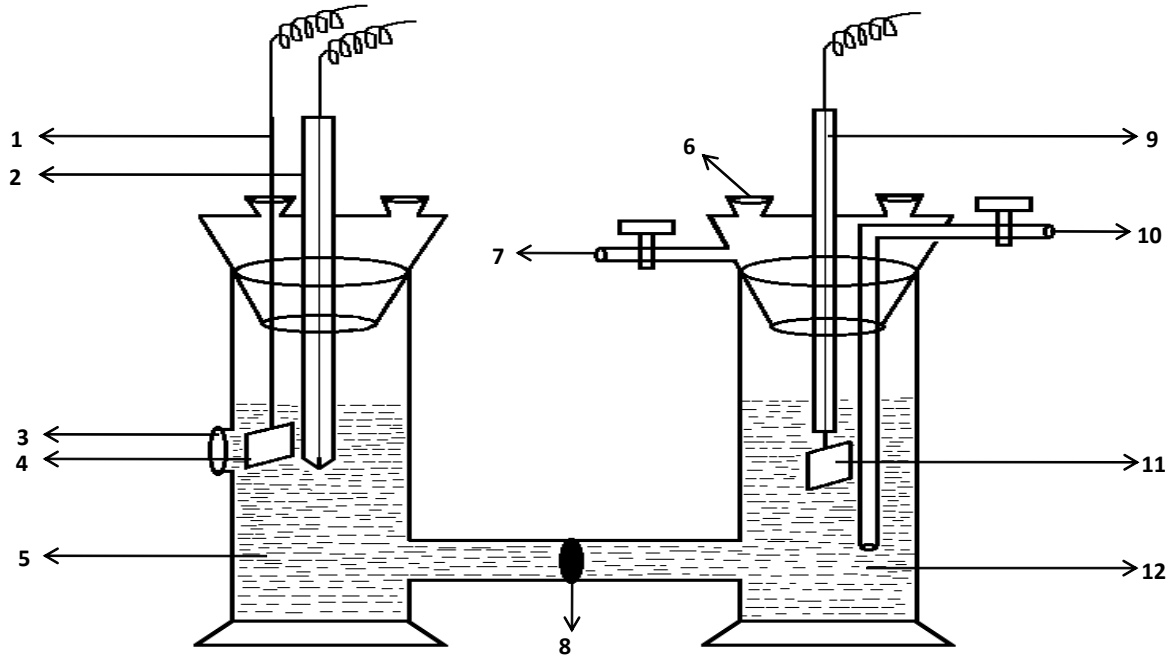

Fig.10 Cell for Photo electro catalytic reduction of CO_2. 1. Working electrode 2. Reference electrode 3.Quartz window 4. SCs coated ITO plate 5. 0.1 M of NaCl .6 Sample valve 7. CO_2 outlet 8. Glass frit 9. Counter electrode 10. CO_2 inlet 11. Pt foil 12. 0.1M $NaHCO_3$/ $KHCO_3$

8.0. STUDIES ON DIFFERENT WORKING ELECTRODES FOR PECR OF CO_2

8.1 Studies on Barium tantalate, $Ba_5Ta_4O_{15}$

8.1.1 XRD patterns

Fig.4.1.1 given below shows the XRD patterns for pure and modified $Ba_5Ta_4O_{15}$.There is no significant change in the XRD pattern of modified $Ba_5Ta_4O_{15}$ with respect to the pristine sample. This could be possibly because of low concentration of the dopants. Crystallite sizes of the pure Ba $_5Ta_4O_{15}$, separately doped with N & S and co-doped with N & Fe samples calculated by using Scherer's equation are given in Table 1. It is observed that on doping with N & Fe crystallites size of the tantalate increases.

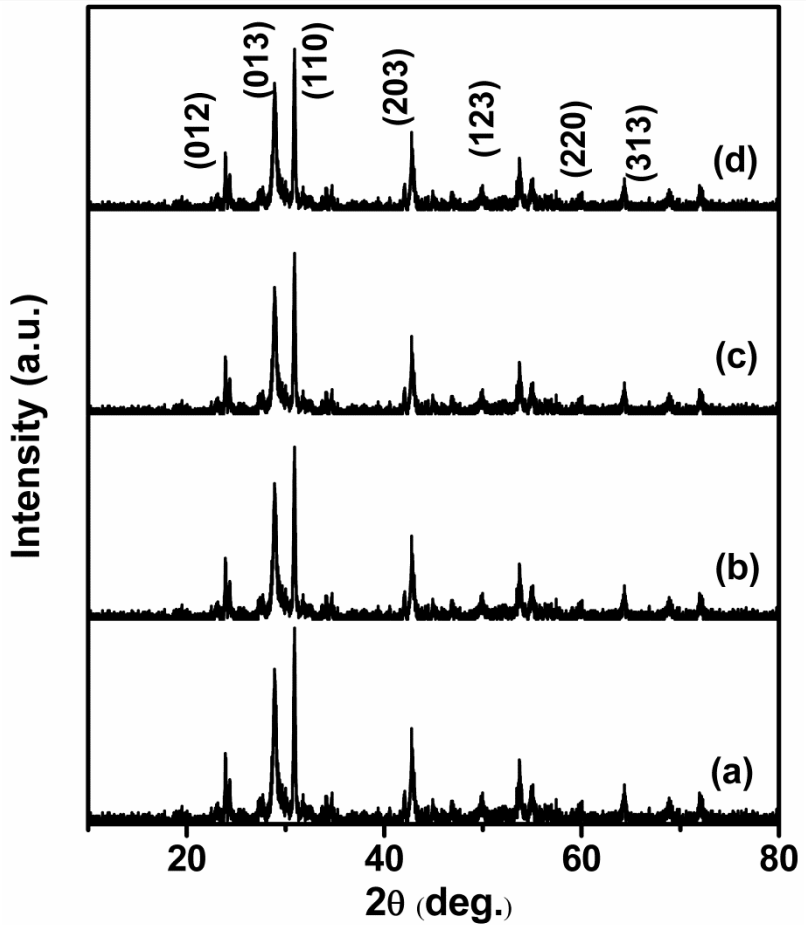

Fig.11 XRD patterns for a. $Ba_5Ta_4O_{15}$ b. N- $Ba_5Ta_4O_{15}$, c. Fe- $Ba_5Ta_4O_{15}$, d. Fe-N/$Ba_5Ta_4O_{15}$

Table .1 Crystallite size and band gap values for pure and modified $Ba_5Ta_4O_{15}$

	Crystalline size (nm)	Band Gap (eV)
$Ba_5Ta_4O_{15}$	63.4	4.2
$NBa_5Ta_4O_{15}$	75.6	3.8
$FeBa_5Ta_4O_{15}$	78.3	3.6
FeN $Ba_5Ta_4O_{15}$	71.7	3.53

8.1.2 SEM studies

Morphology of pristine $Ba_5Ta_4O_{15}$ and Fe, N & Fe-N co-doped samples as revealed by SEM micrographs are presented below.

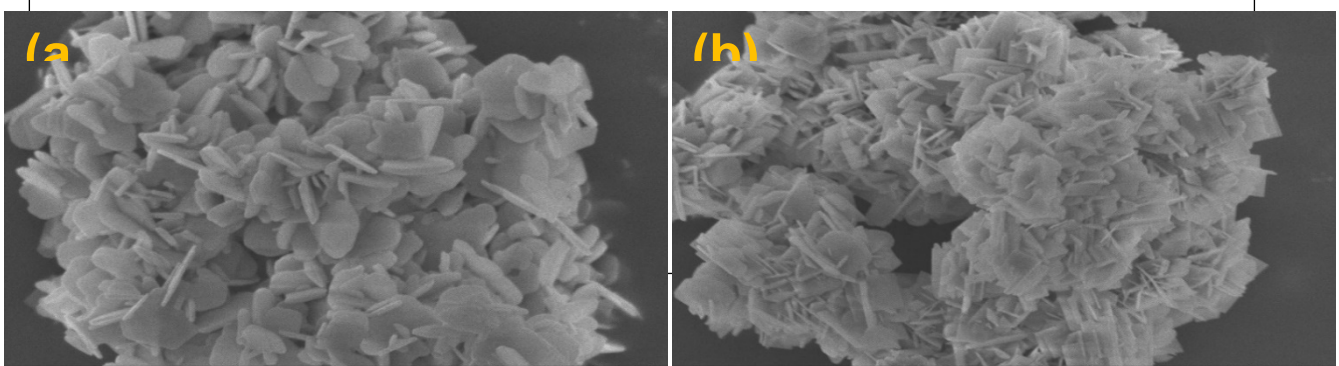

Fig4.1.2 SEM images for a.$Ba_5Ta_4O_{15}$ b. N-$Ba_5Ta_4O_{15}$, c. Fe- $Ba_5Ta_4O_{15}$, d. Fe-N $Ba_5Ta_4O_{15}$

Fig.12 SEM micrographs for a) Pristine, b) N-modified c) Fe modified and d) N & Fe modified $Ba_5Ta_4O_{15}$

Unmodified $Ba_5Ta_4O_{15}$ (Fig. 12a) displays flower like morphology. On modifying pure $Ba_5Ta_4O_{15}$ with N &Fe (Fig. 12b, c & d) no significant change in the flower like structure is observed

8.1.3 Diffuse Reflectance Spectra

Diffuse reflectance spectra for pure and modified $Ba_5Ta_4O_{15}$ in UV-Visible range is shown in the Fig.13. On modification with N & Fe, the light absorption edge shifts towards the visible light region which is reflected in the values of band gap of the modified materials.

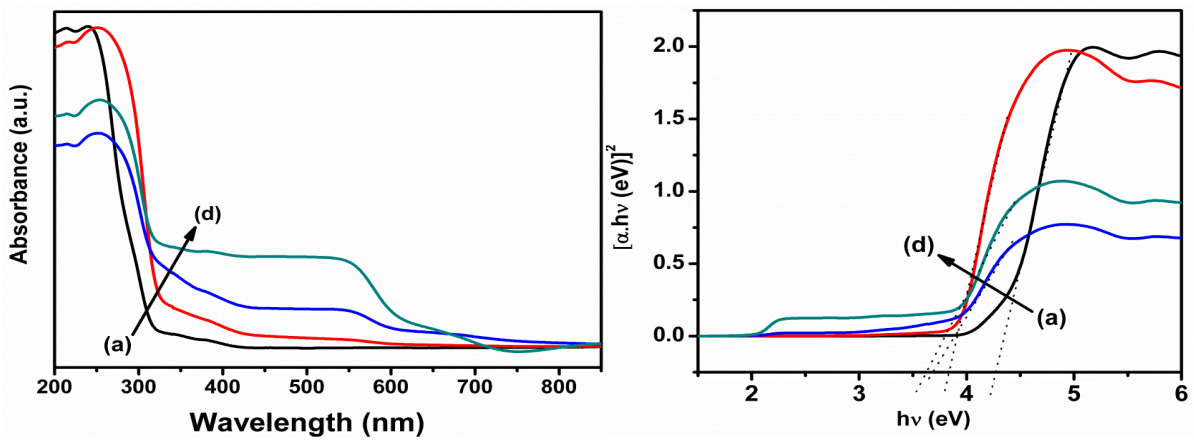

Fig.13. Diffuse reflectance spectra of a.$Ba_5Ta_4O_{15}$ b. N-$Ba_5Ta_4O_{15}$, c. Fe- $Ba_5Ta_4O_{15}$, d. Fe-N $Ba_5Ta_4O_{15}$

The changes in the band gap values calculated by standard method are given in Table 1. Changes in the energy levels of the valence and conduction bands are represented in Fig. 14.

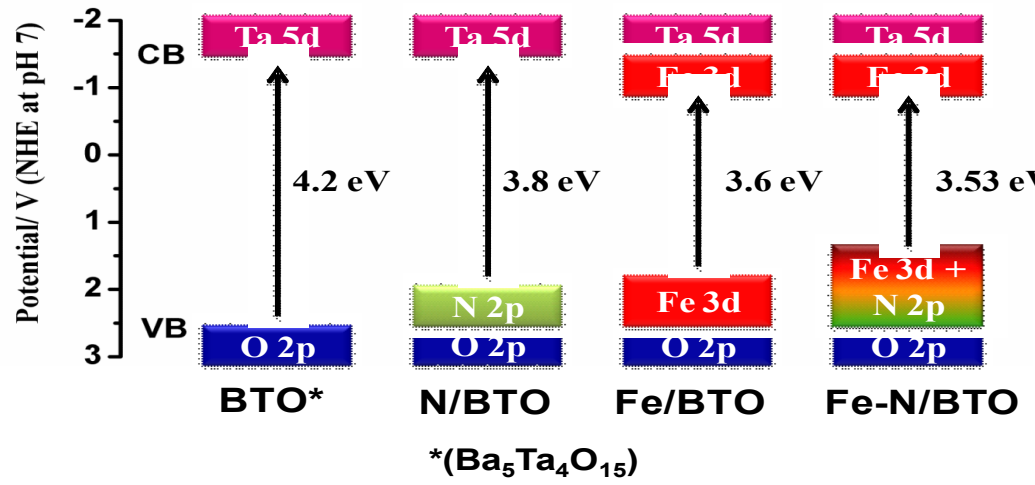

Fig.14. VB & CB energy levels for BTO, N/BTO, Fe/BTO and N- Fe- BTO

8.1.4 Photoluminescence Spectra

Photoluminescence spectra pristine and doped tantalates are shown in Fig.15. With respect to pure $Ba_5Ta_4O_{15}$, all the modified versions show a decrease in the intensity of photoluminescence, indicating a decrease in the charge recombination rates, which in turn, would lead to the longer life of charge carriers.

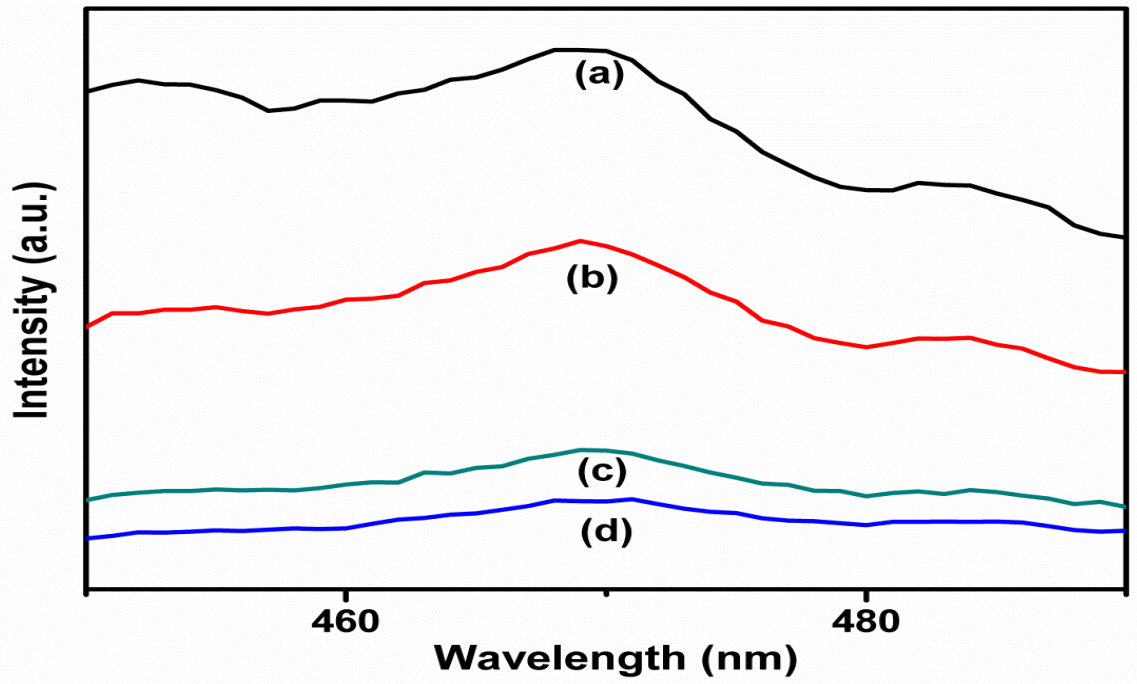

Fig.15 Photoluminescence Spectra of a. $Ba_5Ta_4O_{15}$ b. N-$Ba_5Ta_4O_{15}$, c. Fe- $Ba_5Ta_4O_{15}$, d. Fe-N $Ba_5Ta_4O_{15}$

8.1.5 Photo Electrochemical reduction of CO_2 on $Ba_5Ta_4O_{15}$

Cyclic voltammetry

Given below in Fig.16 is the cyclic voltammetry curves for Fe & N co-doped $Ba_5Ta_4O_{15}$ coated on ITO plate. CV profiles were recorded after purging the electrolyte (0.1M $KHCO_3$) with nitrogen in dark, purging with CO_2 in dark and after illumination with UV-Vis light. CV profile indicates that reduction of CO_2 occurs at the applied potentials of 200 & 600 mv after illumination as well as oxidation reverse sweep (Fig.16). CV profile below clearly indicates the difference when it was in dark and irradiated with light with and without purging of CO_2

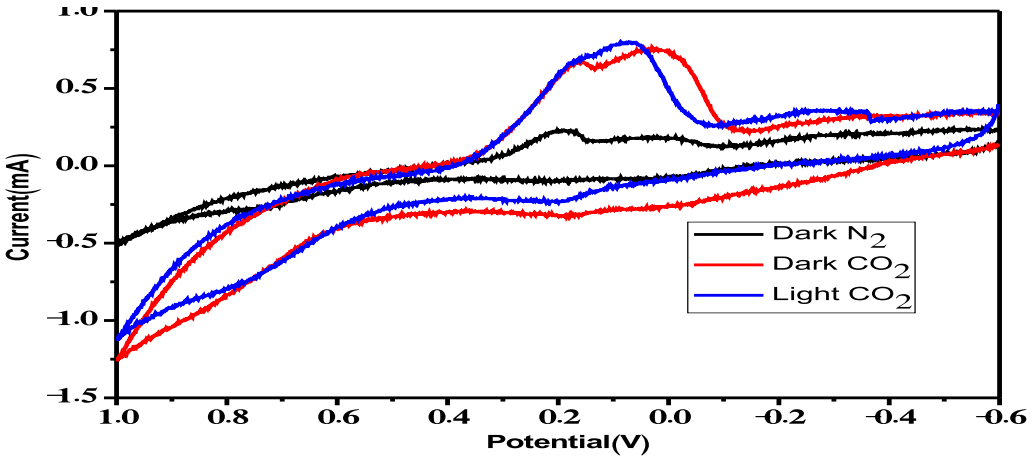

Fig.16 Cyclic voltammetry of FeN/$Ba_5Ta_4O_{15}$with and without purging of CO_2 in 0.1M $KHCO_3$ electrolyte at a scan rate of 10mv/s in the presence and absence of light irradiation.

Linear sweep voltammetry

LSV profile (Fig.17) recorded in the potential range +1V to -2.0V also indicates current generation due to CO_2 reduction occurring at applied voltage of 0.2 V and 0.6 V which is also observed in the CV profile. Hence, CPE measurements were carried out at bias of 0.2V

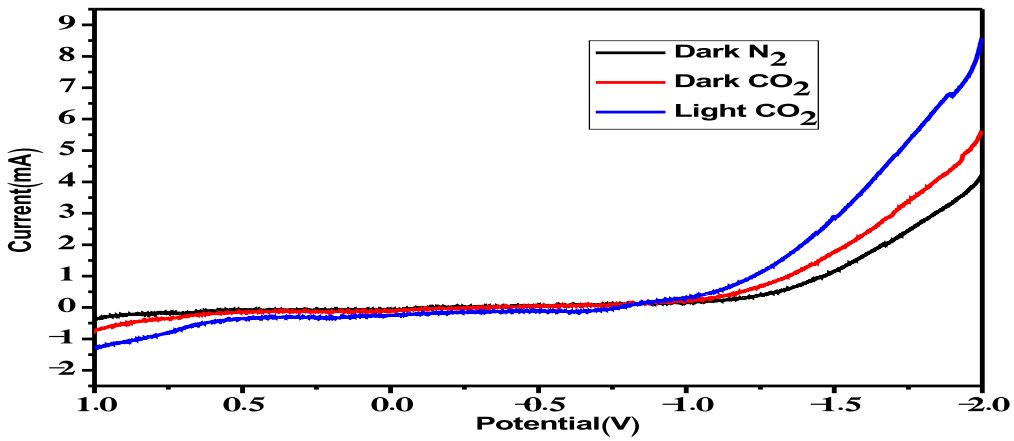

Fig. 17 Linear Sweep voltammetry of $FeN/Ba_5Ta_4O_{15}$ with and without purging of CO_2 in $KHCO_3$ 0.1M Electrolyte at a scan rate of 10mv/s in the presence and absence of light irradiation.

Controlled Potential Electrolysis (CPE)

CPE experiments were performed in three-electrode cell. A Pt foil was used as a counter electrode. The reference electrode was an Ag/AgCl electrode and the working electrode was $FeN/Ba_5Ta_4O_{15}$. At an applied potential of 0.2V V/s Ag/AgCl, the current increases up to 10

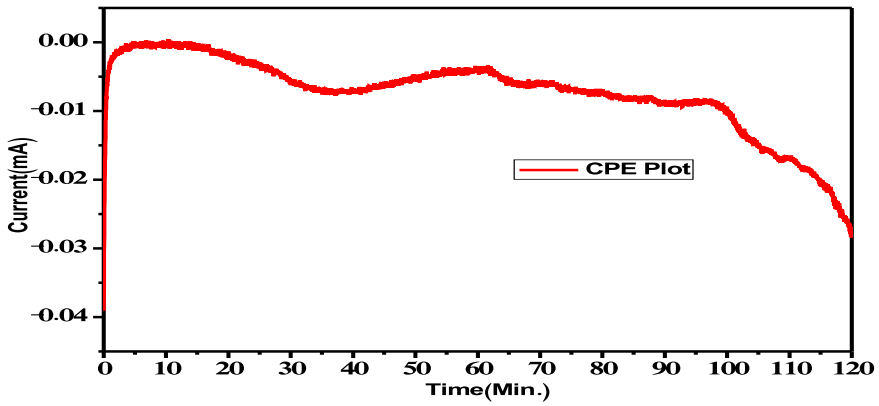

Fig..18 Controlled potential electrolysis with CO2 purging at on potential of 0.2V V/s Ag/AgCl in 0.1M $KHCO_3$electrolyte

min indicating transfer of electrons from anode to cathode (Fig.18). This is due to the oxidation process at anode and after that the current decreases due to the consumption of electrons in carbon dioxide reduction and formation of hydrocarbon products. Corresponding decrease in the quantity of charge is observed in Fig.19. Current and charge quantities at applied voltage of 600 mv are given in Figs.20 and 21 respectively.

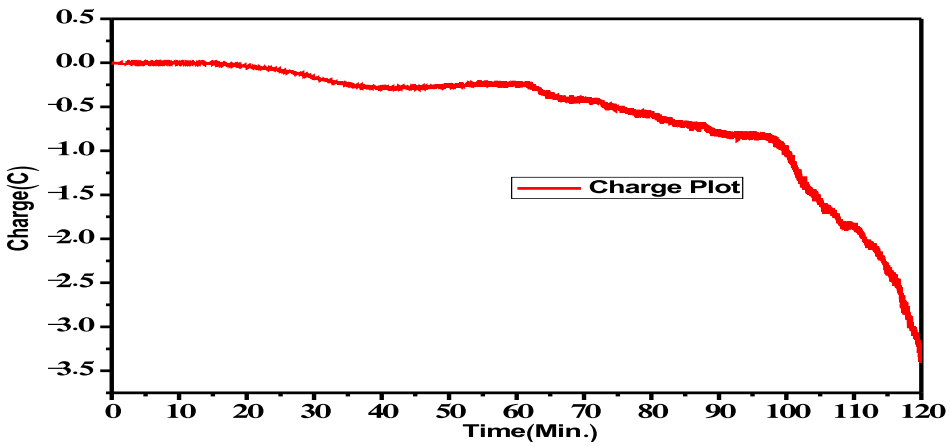

Fig.19 Controlled potential electrolysis charge plot with CO2 purging at on potential of 0.2V V/s Ag/AgCl in 0.1M $KHCO_3$electrolyte

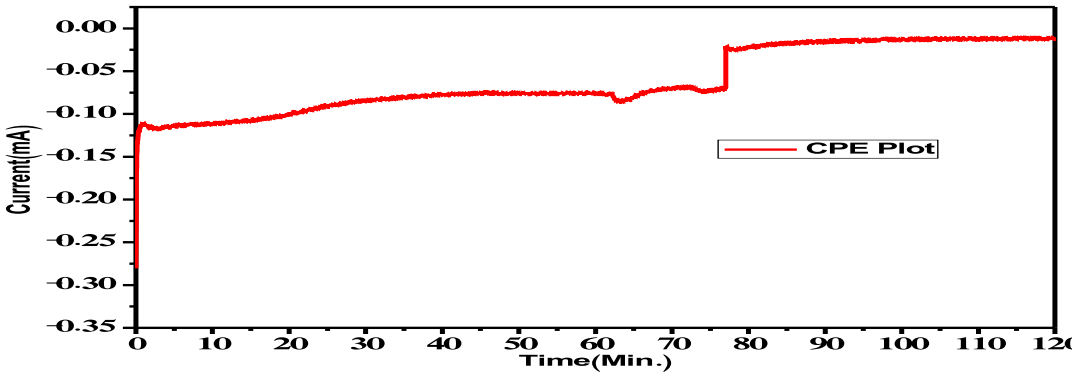

Fig.20 Controlled potential electrolysis with CO2 purging at on potential of 0.6V V/s Ag/AgCl in 0.1M $KHCO_3$electrolyte

Fig.21 Controlled potential electrolysis Charge plot with CO_2 purging at potential of 0.6V V/s Ag/AgCl in 0.1M $KHCO_3$electrolyte

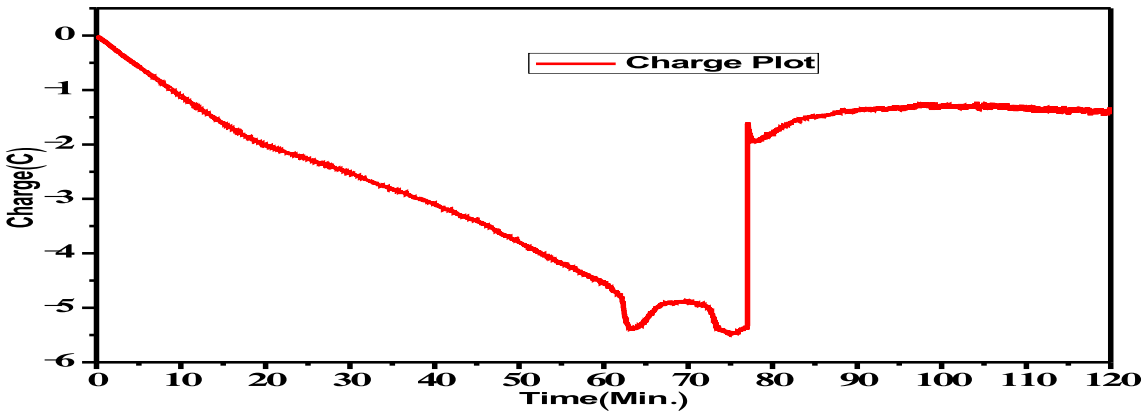

GC analysis of the liquid sample drawn from cathode compartment shows the presence of trace amounts of methanol and ethanol. Quantification was not possible.

8.2. Photo Electrochemical reduction of CO_2 on Fe, N&S doped mesoporous TiO_2

8.2.1 XRD patterns

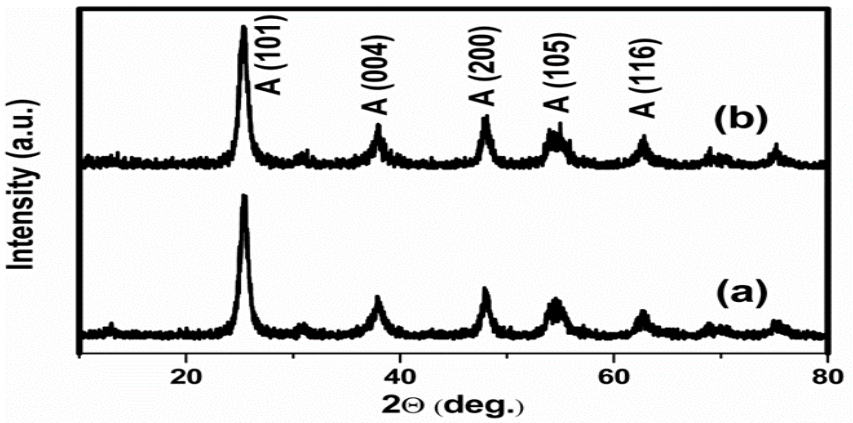

Fig.22 XRD patterns for a. TiO_2, b. $FeNSTiO_2$

Fig.22 given below shows the XRD patterns of neat and modified titanium dioxide Diffraction.

peaks at 2θ values- 25.2 (101), 36.9 (004), 48.0 (200) and 62.7 (204) correspond to anatase phase of prepared FNST [21-23]. In the case of Fe-N-S co-doped TiO_2 (FNST), there is no significant change in XRD patterns when compared to pure TiO_2.This is because of low concentration of dopants

8.2.2 SEM studies

Scanning Electron Micrographs for the neat and modified TiO_2 presented in

Fig.23 shows the spherical morphology for the neat sample. After the modification with Fe ,N & S its crystallite size is reduced.

Adding of dopant precursor during hydrothermal treatment has ensured the incorporation of doped elements into the TiO2 crystal structure. This can be confirmed by the qualitative EDAX spectral data which was shown in Fig.24 EDAX spectra indicate the presence of N, Fe and S in addition of Ti and O elements confirming the doped elements have been incorporated in the synthesized material.

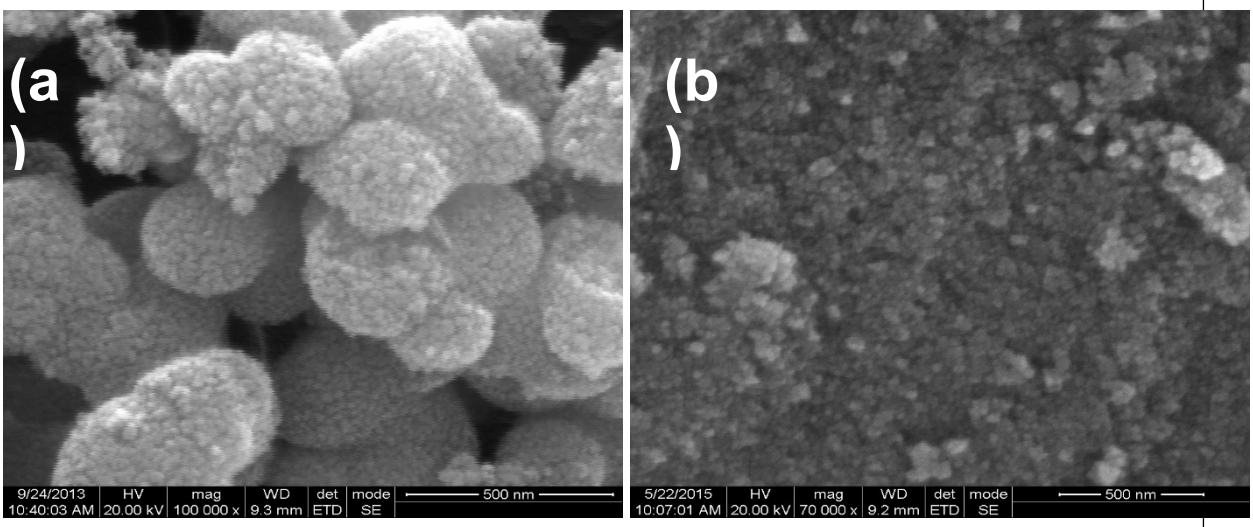

Fig. 23 SEM Results of a. TiO_2, b. $FeNSTiO_2$

8.2.3 UV-Visible Spectra

DRS in UV-Visible region for neat and doped titanium dioxide catalyst are shown in Fig 25 The absorption band edge for FNST is observed at 458 nm which represents the red shifted band edge as compared to pure band edge of TiO2 at 387.5 nm. This can be ascribed to the synergetic effect of Fe-N-S tri-doping, which leads to formation of impurity level between band gap, which is responsible for absorption in visible region

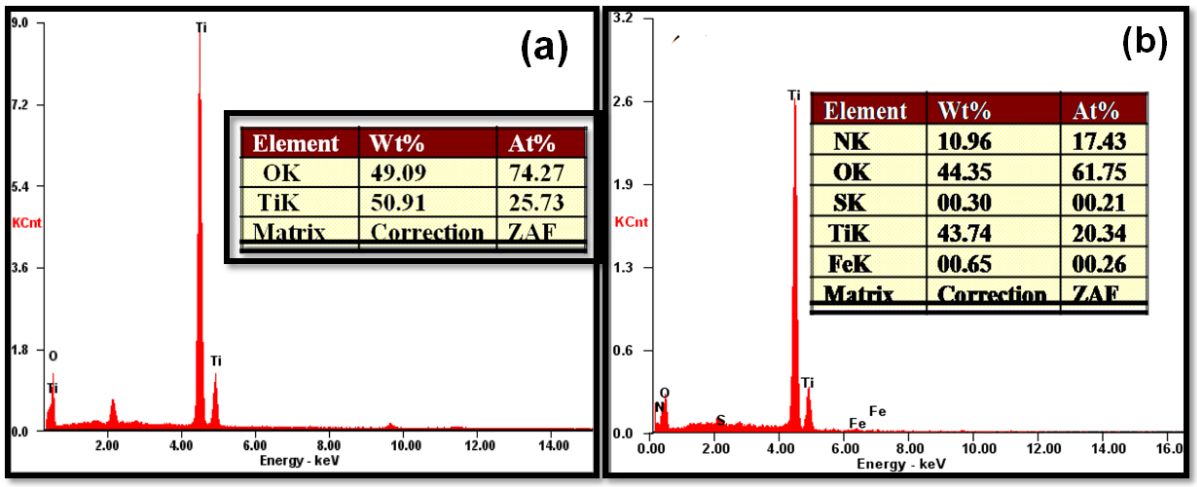

Fig.24. EDAX Spectra of a. TiO_2, b. $FeNSTiO_2$

.

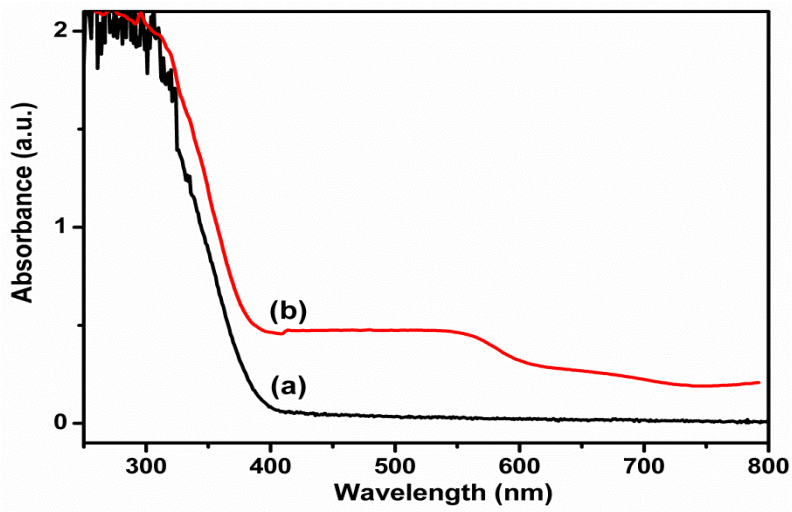

Fig.25 DRS UV-Visible Spectra of a. TiO_2, b. $FeNSTiO_2$

8.2.4 Photoluminescence Spectra

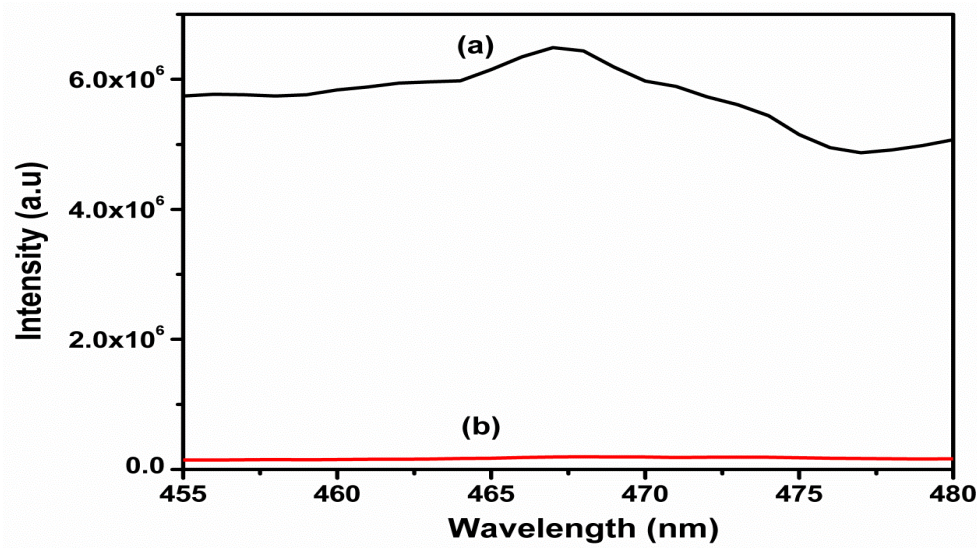

Fig.26 Photoluminescence Spectra of a. TiO_2, b. $FeNSTiO_2$

Photoluminescence studies were carried out to determine the recombination rate of charge carriers. PL emission occurs from the recombination of photo generated electrons and holes. Surface charge transfer and reduced recombination rate of charge carriers and diffusion of reactants are key factors for improving photo catalytic efficiency. Fig.26 below indicates the intensity of modified catalyst is reduced significantly, implying the increase in the life time of the charge carriers.

8.2.5 Cyclic Voltammetry

Cyclic voltammetry profile of the FeNS/TiO_2 (Fig.27) indicates that reduction of CO_2 occurs at the potential of 700 mv as well as oxidation at potential of 100 mv. The profile given below clearly indicates the difference when it was in dark and irradiated with light with and without purging of CO_2

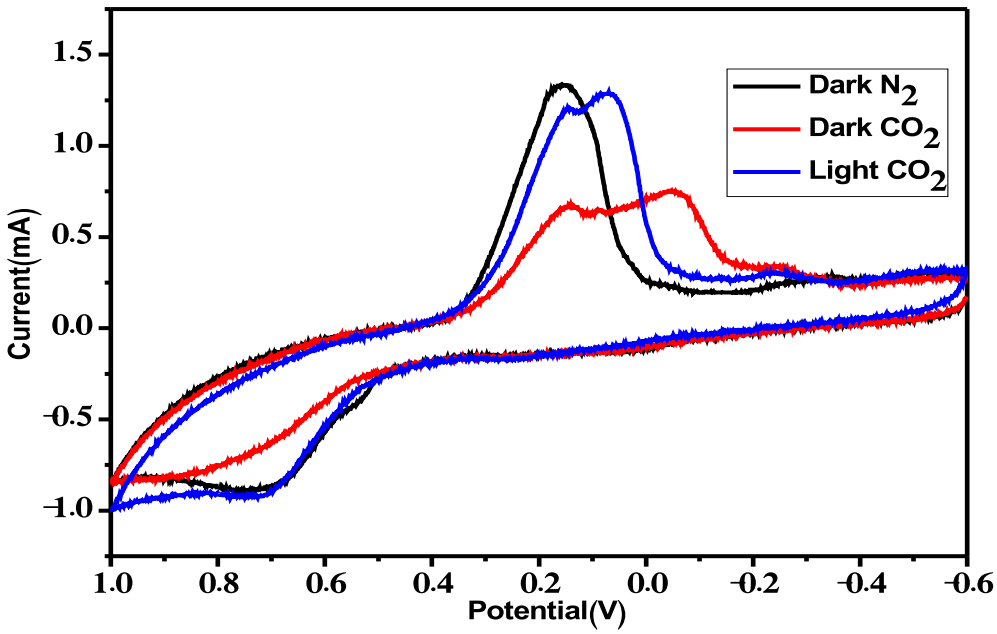

Fig.27 Cyclic voltammetry of FeNS/$TiO_2$with and without purging of CO_2 in $KHCO_3$ 0.1M Electrolyte at a scan rate of 10mv/s in the presence and absence of light irradiation.

8.2.6 Linear Sweep voltammetry

LSV profile given in Fig.28 is the CV profile, indicating CO_2 reduction at an applied voltage of 700 mv resulting in the formation of reduction products.

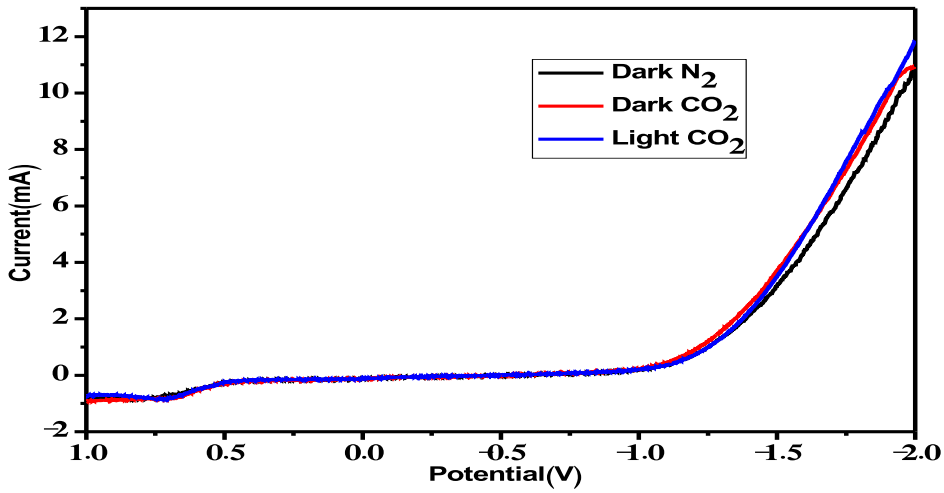

Fig.28 Linear Sweep voltammetry of FeNS/TiO_2 with and without purging of CO_2 in $KHCO_3$ 0.1M Electrolyte at a scan rate of 10mv/s in the presence and absence of light irradiation.

8.2.7 Controlled Potential Electrolysis

CPE experiments were performed in three-electrode cell. A Pt foil was used as a counter electrode. The reference electrode was an Ag/AgCl electrode and the working electrode was

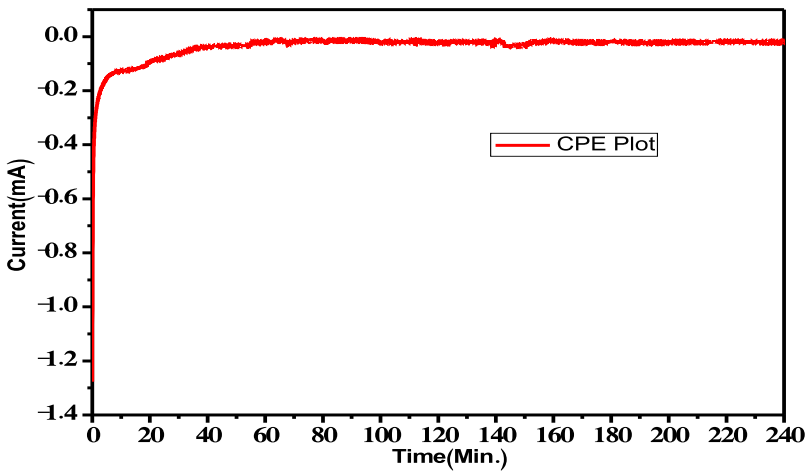

Fig.29 Controlled potential electrolysis with CO_2 purging at on potential of 0.7V V/s Ag/AgCl in 0.1M $KHCO_3$ electrolyte

A potential of 0.7V V/s Ag/AgCl is applied and the current increases up to 40 Min (Fig.29). This is due to the oxidation and after that the current is stabilized this is due to the consumption of electrons during reduction of carbon dioxide and formation of hydrocarbons. Decrease in the charge graph given blow (Fig.30) indicates the formation of hydrocarbon products.

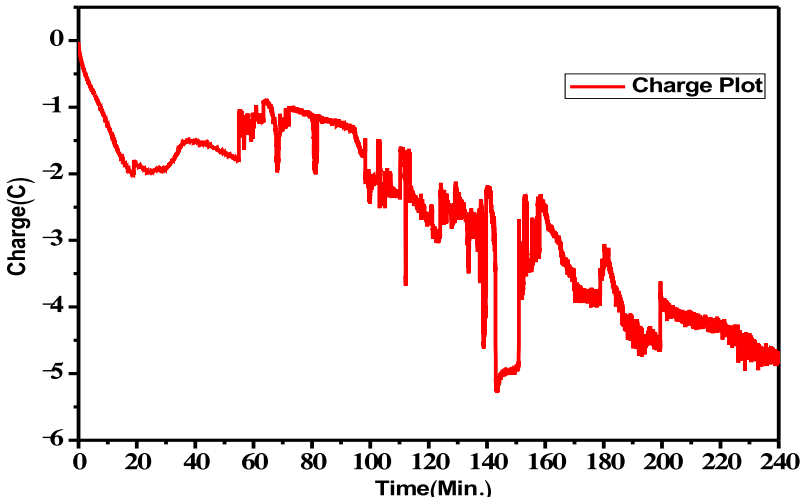

Fig.30 Controlled potential electrolysis charge plot with CO_2 purging at on potential of 0.7V V/s Ag/AgCl in 0.1M $KHCO_3$ electrolyte

GC analysis of the liquid sample from cathode compartment indicated the presence of trace amount of methanol.

8.3. Fe-N modified $Na_{(1-x)}$ $La_xTaO_{(3+x)}$

8.3.1 XRD pattern

X- Ray Diffraction (XRD) studies were carried out to investigate the changes in the structure of $NaTaO_3$ after doping with different elements. XRD patterns for the synthesized materials are shown in Fig. 31 Peaks at 2Θ values of 22.9(020),

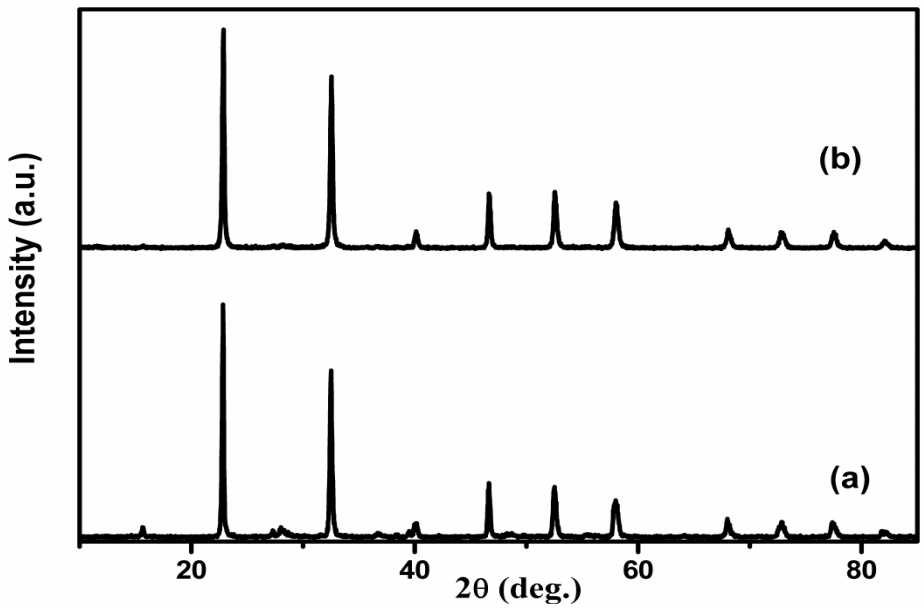

Fig.31 XRD pattern for neat and modified catalyst a. NaTaO3, b. Fe-N/ Na(1-x)LaxTaO(3+x)

32.5(200), 40.1(022), 46.6(202), 52.4(301), 58.2(123) correspond to orthorhombic crystal structure (JCPDS Card No. 25-0863) of $NaTaO_3$. There is no significant change in XRD patterns with co-doped catalysts and no diffraction peaks related to La_2O_3, Fe_2O_3, Ta_2O_5 were found.

8.3.2 SEM Results

Morphology and elemental composition of the synthesized catalysts has been established by SEM and EDXA studies. Fig. 32 and Fig. 33 show SEM images for the neat NaTaO3 and Fe-N modified La doped NaTaO3 catalysts. SEM image clearly reveals that cubic morphology is retained with modified photo catalyst.

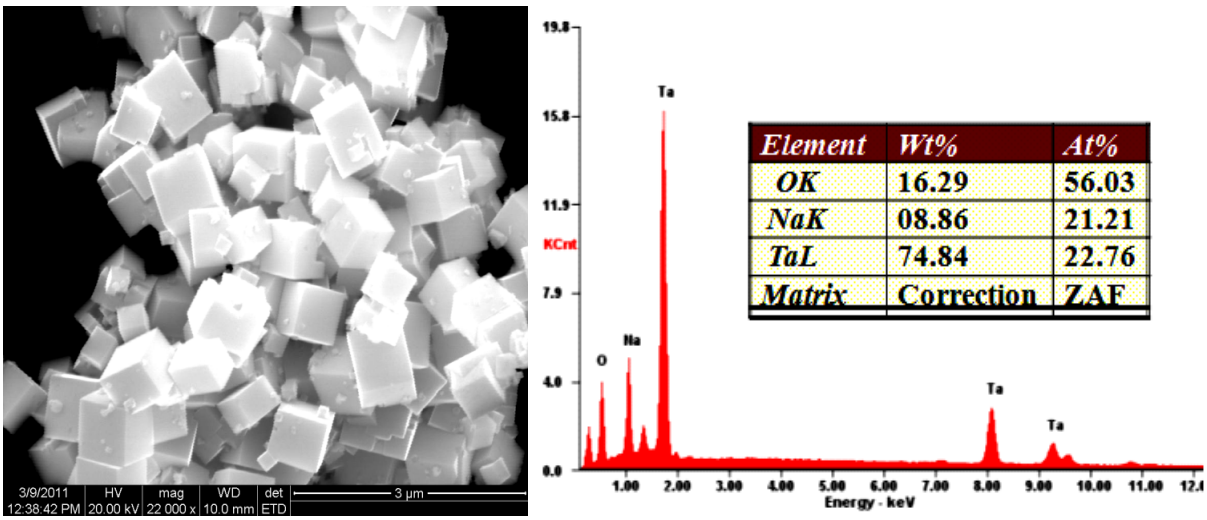

Element	Wt%	At%
OK	16.29	56.03
NaK	08.86	21.21
TaL	74.84	22.76
Matrix	Correction	ZAF

Fig.32SEM image and EDXA spectrum for $NaTaO_3$ photo catalyst

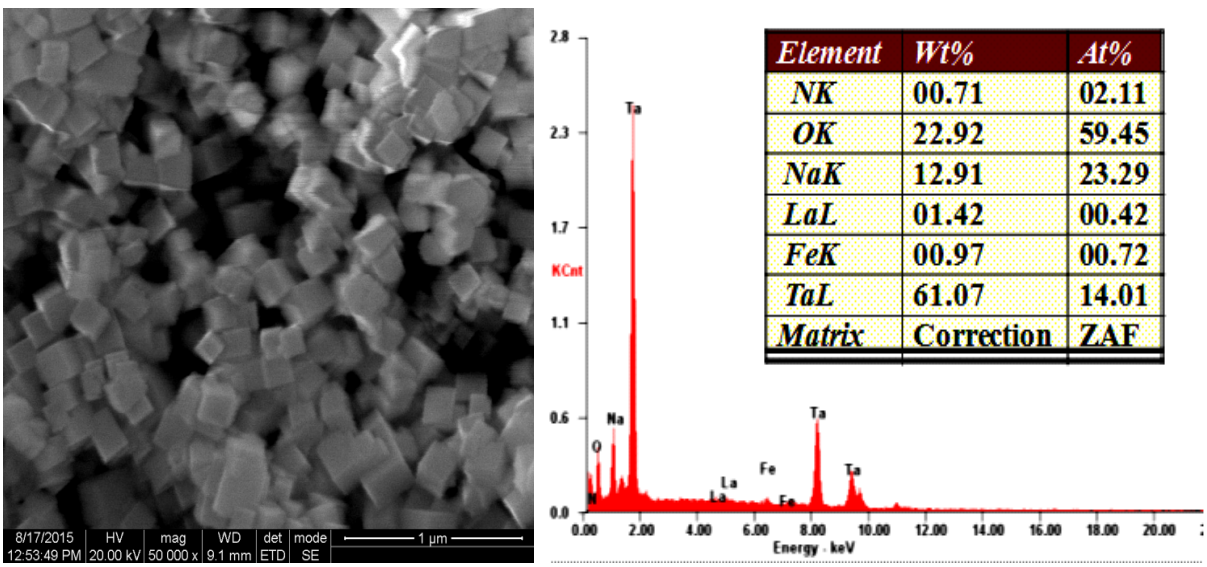

Element	Wt%	At%
NK	00.71	02.11
OK	22.92	59.45
NaK	12.91	23.29
LaL	01.42	00.42
FeK	00.97	00.72
TaL	61.07	14.01
Matrix	Correction	ZAF

Fig.33 SEM image and EDXA spectrum for Fe-N/$Na_{(1-x)}La_xTaO_{(3+x)}$ photo catalyst

8.3.3 UV-Visible Spectra

DRS spectra in UV-Visible region of the pure and modified $NaTaO_3$ catalysts are shown in

Fig.34. Absorption edge for pure $NaTaO_3$ is at 310 nm, ie., only in UV region with a band gap of 4.0 eV. It is apparent that the DR spectra for the modified catalyst showed red shift towards the visible region.

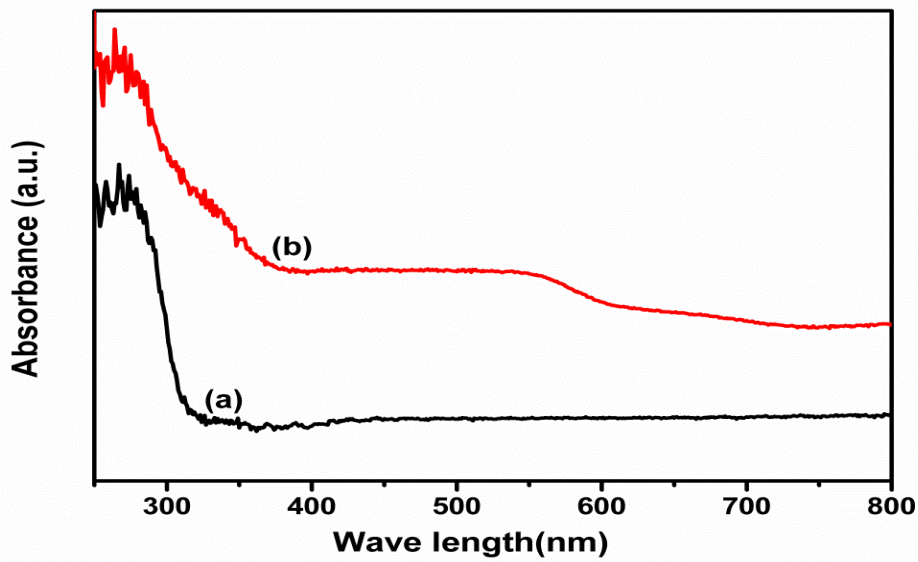

Fig. 34 Diffuse reflectance spectra of neat and modified $NaTaO_3$ catalystsa. $NaTaO_3$, b. Fe-N/ Na(1-x)LaxTaO(3+x).

8.3.4 Photoluminescence Spectra

Photoluminescence spectra for the neat and modified catalysts are shown in Fig.35. An

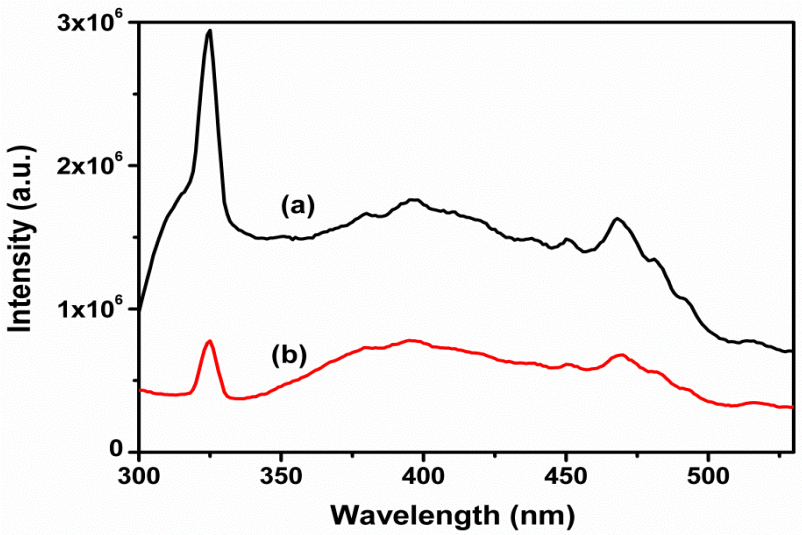

Fig. 35. Photo luminescence spectra for neat and modified $NaTaO_3$ catalystsa. $NaTaO_3$, b. Fe-N/ Na(1-x)LaxTaO(3+x)

emission peak at 469 nm is observed for the neat and modified NaTaO3, indicating that doping of catalyst does not result in any new PL spectral line, but the intensity of the line is reduced. PL spectra mainly result from the recombination of charge carriers and its intensity is directly proportional to the probability of the recombination of charge carriers. There is a sharp decrease in the intensity with co-doping of catalyst, which is expected to reduce the charge carriers recombination rates.

8.3.5 Cyclic Voltammetry

Given below in Fig.36 is the cyclic voltammetry profiles for Fe-N/Na(1-x) Lax TaO(3+x) which indicates that reduction of CO_2 occurs at the potentials of 500&700 mv as well as oxidation occurs at potential of 100mv The figure given below clearly indicates the difference when it was in dark and irradiated with light with and without purging of CO_2

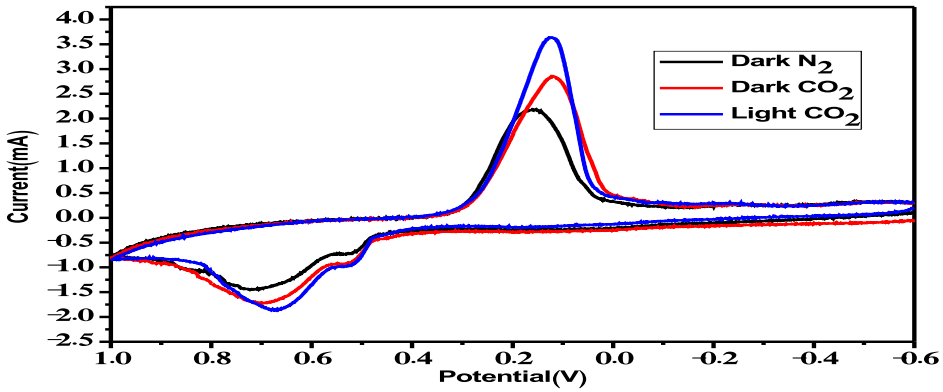

Fig.36 Cyclic voltammetry of FeN/ Na(1-x)LaxTaO(3+x) with and without purging of CO_2 in $NaHCO_3$ +$NaCO_3$ 0.1M Electrolyte at a scan rate of 10mv/s in the presence and absence of light irradiation.

8.3.6 Linear Sweep voltammetry

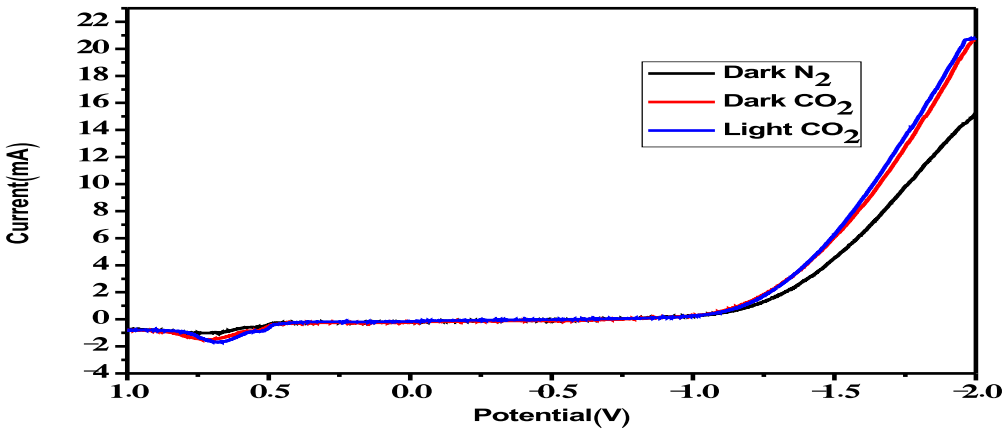

Fig.37 Linear Sweep voltammetry of FeN/ Na(1-x)LaxTaO(3+x) with and without purging of CO_2 in $NaHCO_3$ +$NaCO_3$ 0.1M Electrolyte at a scan rate of 10mv/s in the presence and absence of light irradiation.

LSV profile (Fig) for the catalyst is in line with the reduction pattern observed in CV profile, indicating CO_2 reduction processes at applied voltage of 500 & 700 mv. The steep increase in current at - 1.2 V is due to hydrogen evolution by splitting of water.

8.3.7 Controlled Potential Electrolysis

CPE experiments were performed in three-electrode cell. A Pt foil was used as a counter electrode. The reference electrode was an Ag/AgCl electrode and the working electrode was

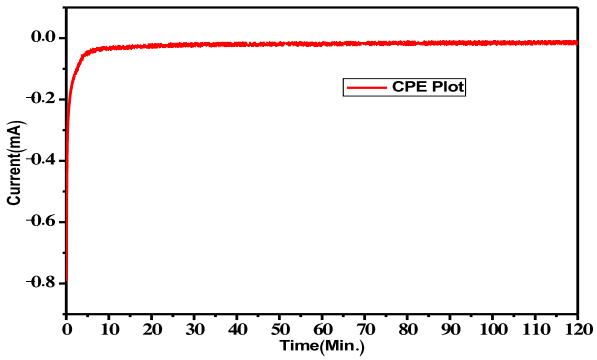

Fig.38 Controlled potential electrolysis with CO_2 purging at on potential of 0.5V V/s Ag/AgCl in $NaHCO_3$ +$NaCO_3$ 0.1M Electrolyte

.At an applied potential of 0.5V V/s Ag/AgCl the current increases up to 10Min. (Fig.38) due to the oxidation and after that the current is stabilized indicating consumption of electron for reduction of carbon dioxide and formation of hydrocarbons. Decrease in the charge graph given blow (Fig.39) indicates the formation of hydrocarbons.

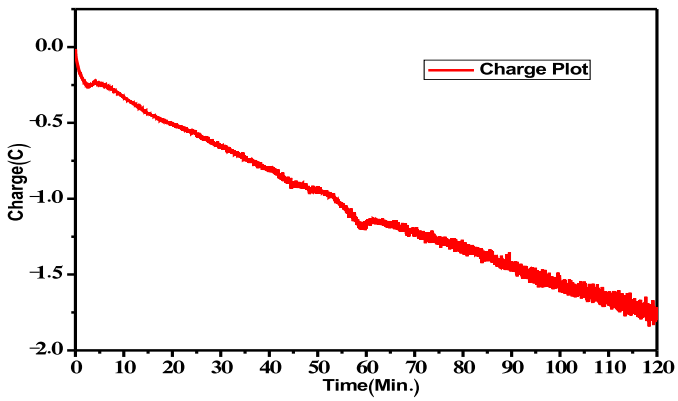

Fig.39 Controlled potential electrolysis Charge plot with CO_2 purging at on potential of 0.5V V/s Ag/AgCl in $NaHCO_3$ +$NaCO_3$ 0.1M Electrolyte

8.4 $Sr_3Ti_2O_7$ doped with N, S & Fe

8.4.1 XRD pattern

X-ray diffraction patterns for prepared layered strontium titanate photo catalysts in pure and doped forms are shown in Fig.40. All the characteristic d-lines for $Sr_3Ti_2O_7$ phase are observed in the XRD patterns for neat and doped samples. The amount of dopants being small, no major changes in the XRD patterns for the doped samples are observed.

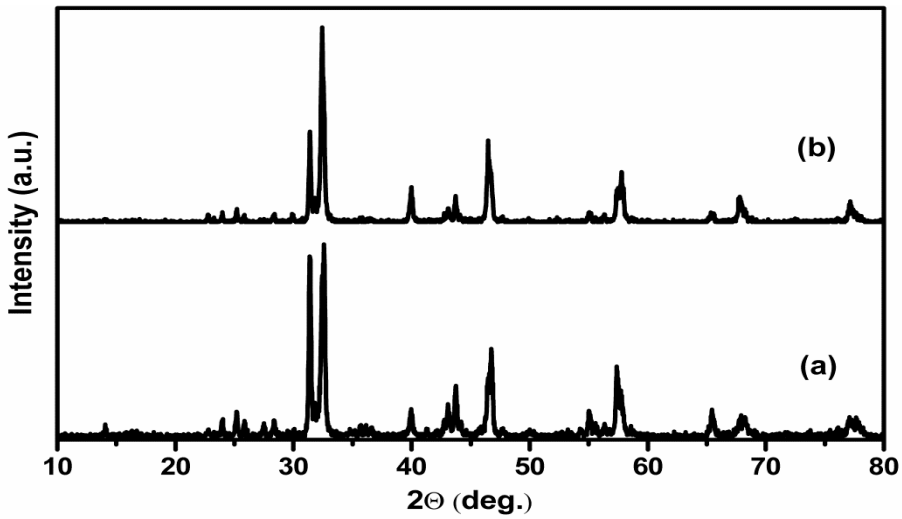

Fig. 40 XRD patterns for neat and doped $Sr_3Ti_2O_7$a. $Sr_3Ti_2O_7$, b. FeNS $Sr_3Ti_2O_7$

8.4.2 SEM Results& EDAX Spectra

SEM for the neat $Sr_3Ti_2O_7$ as shown in Fig.41a reveals a distinct plate like morphology. Doping with N, S and Fe brings out significant changes in the morphology and size of the crystal is decreased (Fig.41b) The incorporation of the dopants is confirmed by EDAX Spectra and the qualitative data in Fig.42 are given below

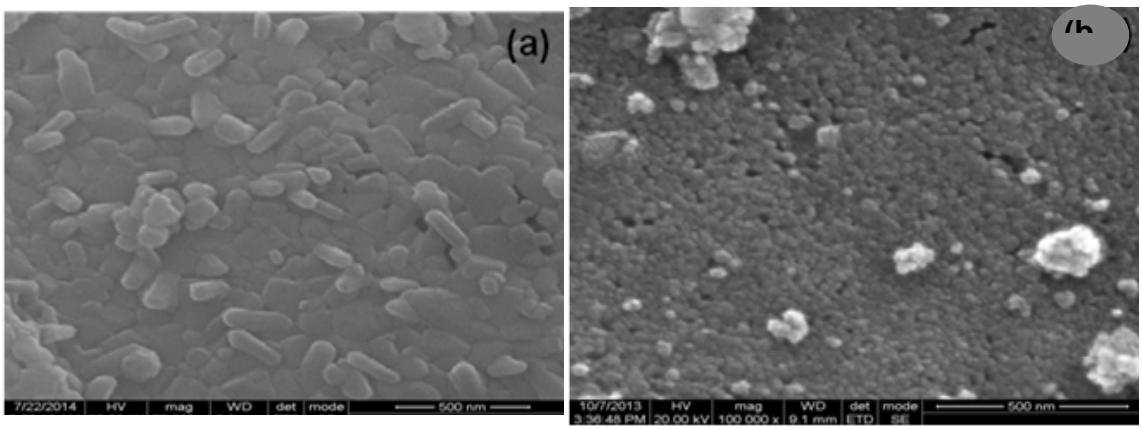

Fig.41 SEM image of pure and doped a. $Sr_3Ti_2O_7$, b. FeNS $Sr_3Ti_2O_7$

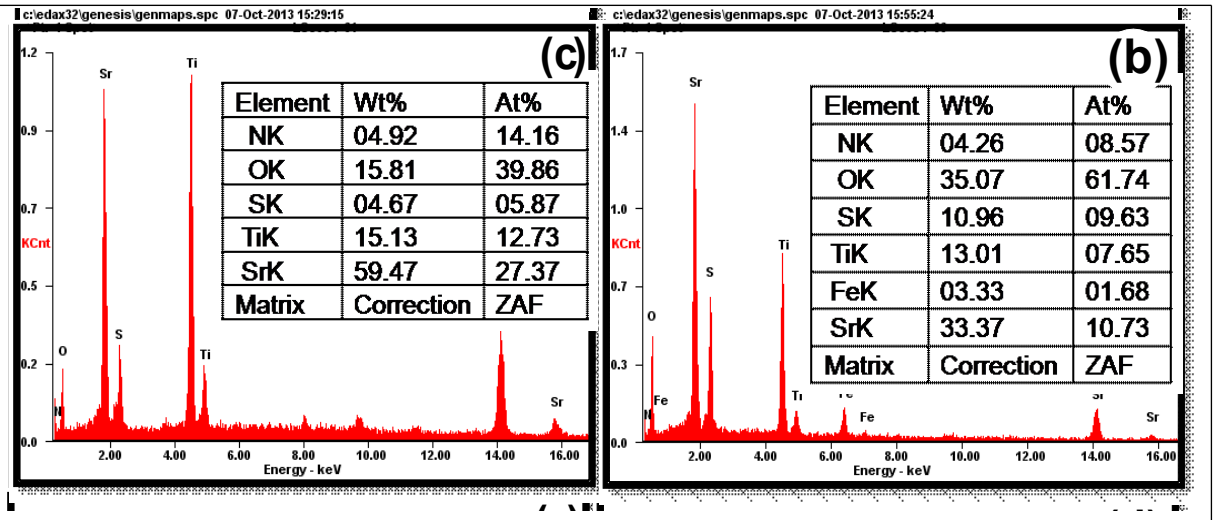

Fig.42 EDAX Spectra of a. $Sr_3Ti_2O_7$, b. FeNS $Sr_3Ti_2O_7$

8.4.3 DRS UV-Visible Spectra

DRS profiles for neat and Fe-N-S co-doped samples as shown in Fig.43 indicate that on co-doping, the adsorption edge turns into a near continuum, extending deeper into the visible region, due to excitations from two different energy levels within the band gap

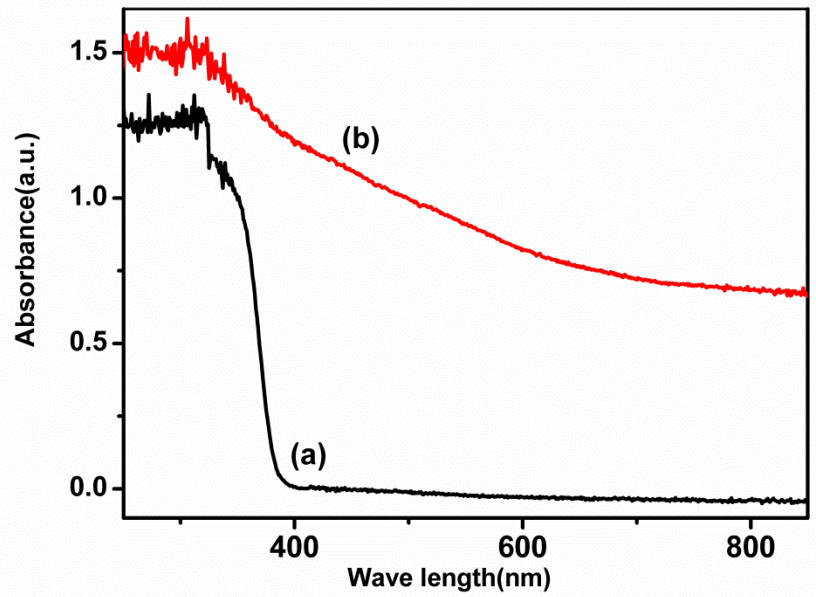

Fig. 43 Diffuse Reflectance spectra for neat and doped Sr3Ti2O7 catalysts. a. $Sr_3Ti_2O_7$, b. FeNS $Sr_3Ti_2O_7$

8.4.4 Photoluminescence Spectra

Photo luminescence spectra of the catalysts (Fig.44) bring out additional features of doped catalysts. Undoped $Sr_3Ti_2O_7$ shows two photo luminescence (PL) emission lines at 470 nm and 482 nm with significant intensity, arising due to the recombination of charge carriers. However, on co-doping with Fe and N-S, sharp reduction in

intensity of the PL lines is observed. Decrease in the intensity of PL lines indicates that the recombination of charge carriers is retarded in presence of the dopants. Such an effect would lead to an increase in the life time of the photo generated electrons and holes and hence, an increase in PCRC activity.

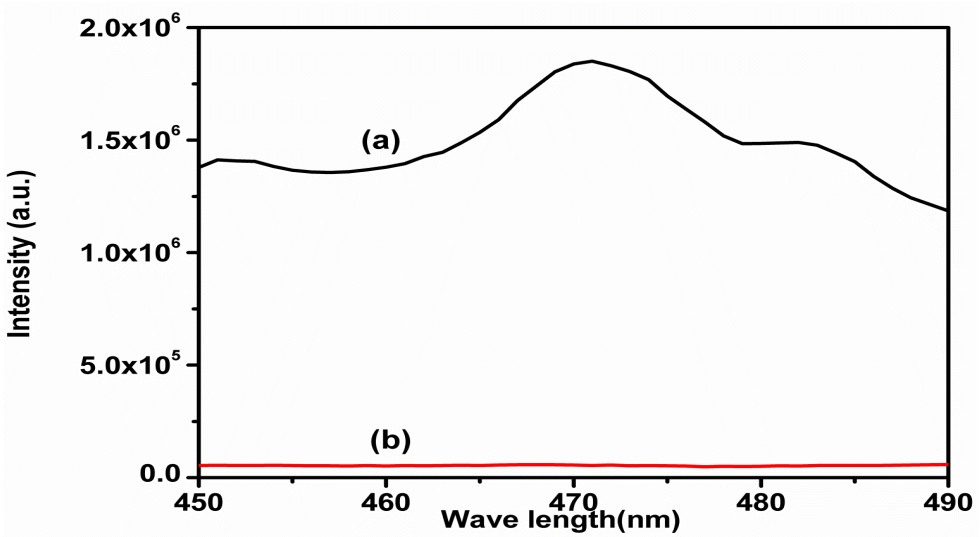

Fig. 44. Photo luminescence spectra for neat and doped Sr3Ti2O7 catalysts. a. $Sr_3Ti_2O_7$, b. FeNS $Sr_3Ti_2O_7$

8.4.5 Cyclic voltammetry

Given below in Fig.4.4.5a and Fig.4.4.5b are cyclic voltammetry profiles for Fe-N-S co-doped $Sr_3Ti_2O_7$ which indicates that reduction of CO_2 occurs at the potentials of 560 &700 mv as well as oxidation at potential of 140 mv.. The profile clearly indicates the difference when it was in dark and irradiated with light with and without purging of CO_2

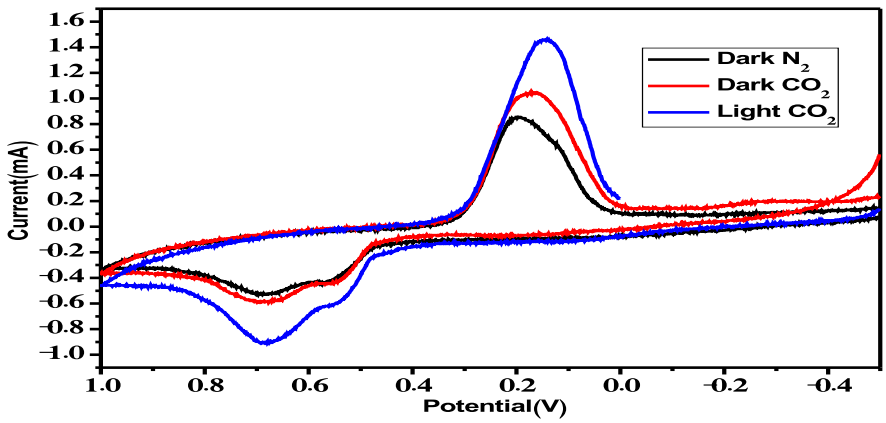

Fig.45 Cyclic voltammetry of FeNS/ $Sr_3Ti_2O_7$ with and without purging of CO_2 in $NaHCO_3$ +$NaCO_3$ 0.1M Electrolyte at a scan rate of 10mv/s in the presence and absence of light irradiation.

8.4.6 Linear Sweep Voltammetry

LSV profile shown in Fig. 46 also indicates two reduction processes at applied potentials, 500 & 700 mv, thus confirming the observations in CV profile.

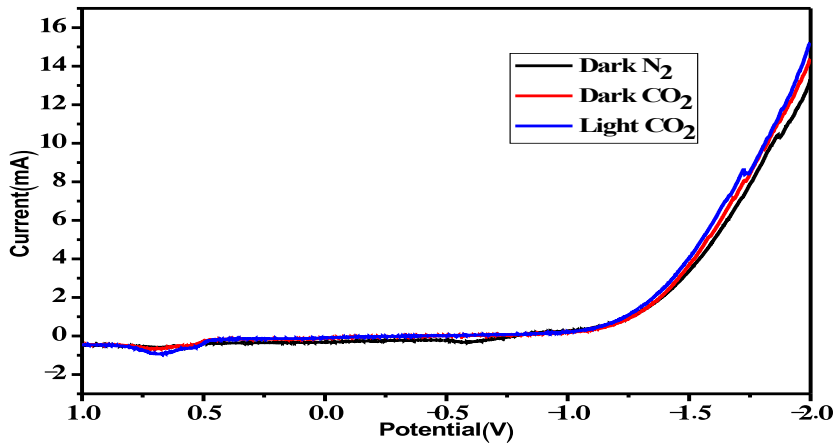

Fig.46 Linear Sweep Voltammetry of Fe-N-S/ $Sr_3Ti_2O_7$ with and without purging of CO_2 in $NaHCO_3$ +$NaCO_3$ 0.1M Electrolyte at a scan rate of 10mv/s in the presence and absence of light irradiation.

8.4.7 Controlled Potential Electrolysis

CPE experiment was performed in three-electrode cell. A Pt foil was used as a counter electrode. The reference electrode was an Ag/AgCl electrode and the working electrode was FeNS/$Sr_3Ti_2O_7$. A bias potential of 0.6V V/s Ag/AgCl is applied. Current due to electron transfer to cathode increases up to 5Min. due to the oxidation and after that the current is

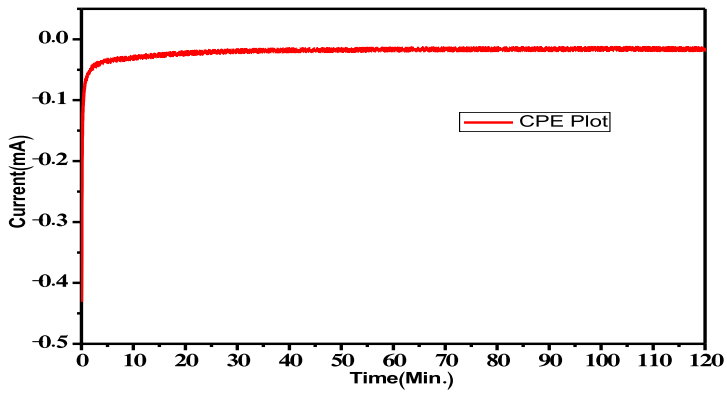

Fig.47 Controlled potential electrolysis with CO_2 purging at on potential of 0.6V V/s Ag/AgCl in $NaHCO_3$ +$NaCO_3$ 0.1M Electrolyte

stabilized, due to consumption of electron in the reduction of carbon dioxide and formation of hydrocarbons (Fig.47). Decrease in the charge graph given blow (Fig.48) indicates the formation of hydrocarbon derivatives

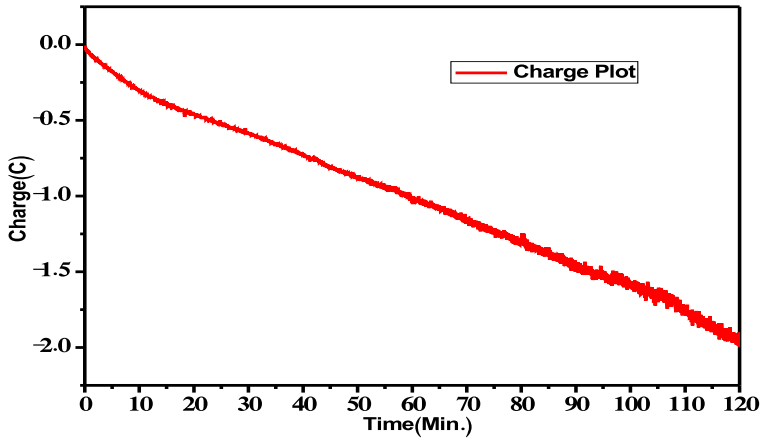

Fig.48 Controlled potential electrolysis Charge plot with CO_2 purging at on potential of 0.6V V/s Ag/AgCl in $NaHCO_3$ +$NaCO_3$ 0.1M Electrolyte

GC analysis of the liquid samples from the cathode compartment indicated the presence of trace amounts of methanol

8.5 CuPc sensitized $Sr_3Ti_2O_7$

8.5.1 XRD patterns

X-ray diffraction patterns for prepared layered strontium titanate photo catalysts in pure and doped forms are shown in Fig.49 All the characteristic d-lines for $Sr_3Ti_2O_7$phase are

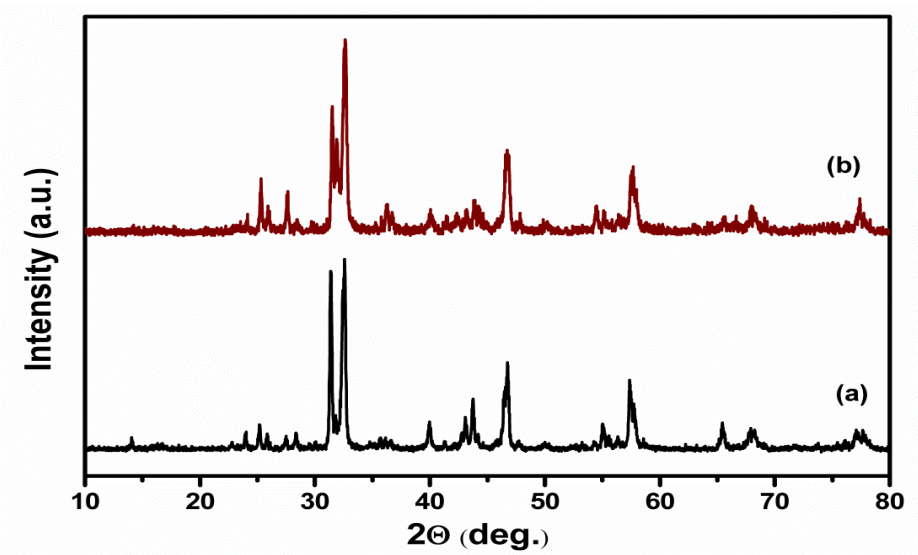

Fig. 49 XRD patterns for neat and doped $Sr_3Ti_2O_7$a. $Sr_3Ti_2O_7$, b. CuPc $Sr_3Ti_2O_7$

Sensitization of $Sr_3Ti_2O_7$

observed in the XRD patterns for neat and doped samples. The amount of dopants being small, no major changes in the XRD patterns for the doped samples are observed

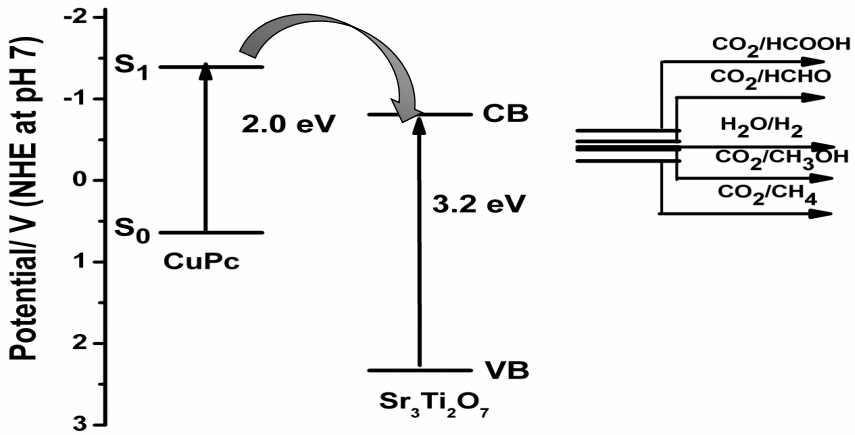

Fig.50. Band position for neat and doped $Sr_3Ti_2O_7$ a. $Sr_3Ti_2O_7$, b. CuPc $Sr_3Ti_2O_7$

Since the band gap of pristine $Sr_3Ti_2O_7$ is 3.2 eV, it is a wide band semi-conductor, active in the UV region only. In order to improve the efficiency of light absorption, it is sensitized with Copper phthalocyanin, which is a short band semi-conductor, active in the visible region. Sensitization as shown in Fig.50 results in the transfer of photo electrons from the CB of CuPc to the CB of the titanate, thus improving the photo catalytic efficiency

8.5.2 Cyclic voltammetry

Given below in Fig.51is cyclic voltammetry of the CuPc/$Sr_3Ti_2O_7$ which indicates that reduction of CO_2 occurs at the potential of 500 & 700mv as well as oxidation occurs at potential of 180mv.the figure given below clearly indicates the difference when it was in dark and irradiated with light with and without purging of CO_2

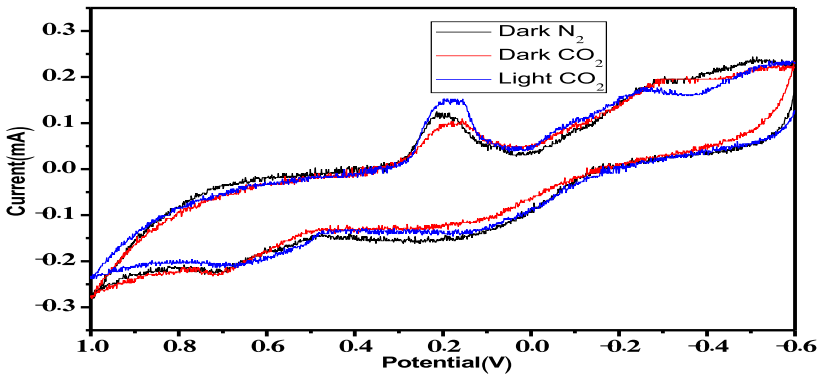

Fig.51 Cyclic voltammetry of CuPc/$Sr_3Ti_2O_7$ with and without purging of CO_2 in $NaHCO_3$ +$NaCO_3$ 0.1M Electrolyte at a scan rate of 10mv/s in the presence and absence of light irradiation.

8.5.3 Linear sweep voltammetry

LSV profile as given in Fig.52 also indicates reduction processes at applied potential of 500 and 700 mv, which is in line with the CV profile.

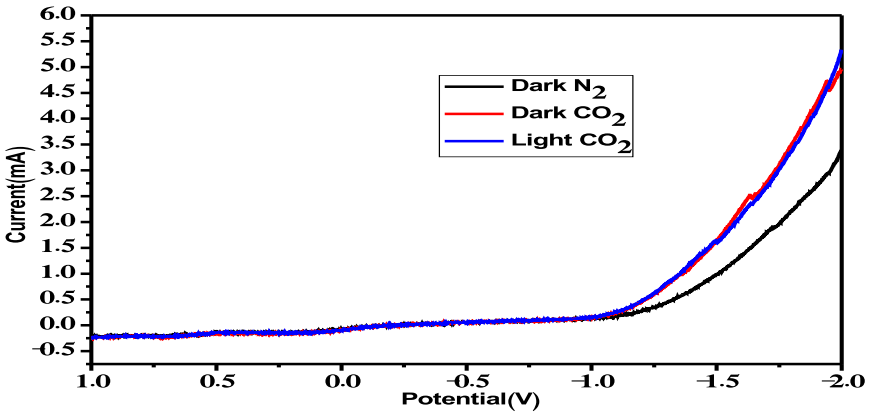

Fig.52 Linear Sweep voltammetry of CuPc/$Sr_3Ti_2O_7$ with and without purging of CO_2 in $NaHCO_3$ +$NaCO_3$ 0.1M Electrolyte at a scan rate of 10mv/s in the presence and absence of light irradiation.

8.5.4 Controlled potential Electrolysis

CPE experiments (Fig.53) were performed in three-electrode cell. A Pt foil was used as a counter electrode. The reference electrode was an Ag/AgCl electrode and the working electrode was CuPc/$Sr_3Ti_2O_7$.The potential of 0.6V V/s Ag/AgCl is applied the current is increase up to 5Min due to the oxidation and after that the current is stabilized due to consumption of electrons for reduction of carbon dioxide and formation of hydrocarbons. Decrease in the charge graph given blow (Fig.54) indicates the formation of hydrocarbons.

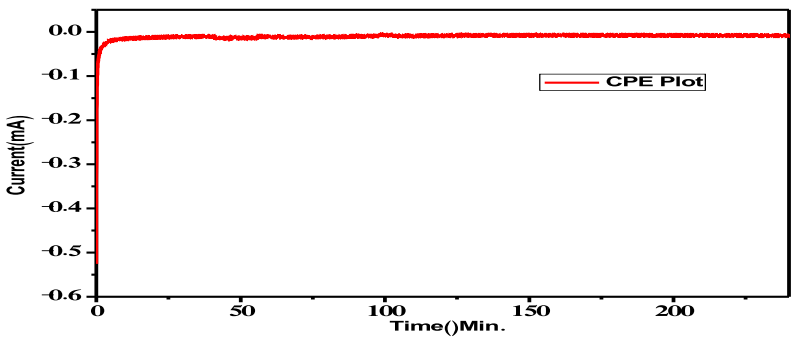

Fig.53 Controlled potential electrolysis with CO_2 purging at on potential of 0.6V V/s Ag/AgCl in $NaHCO_3$ +$NaCO_3$ 0.1M Electrolyte

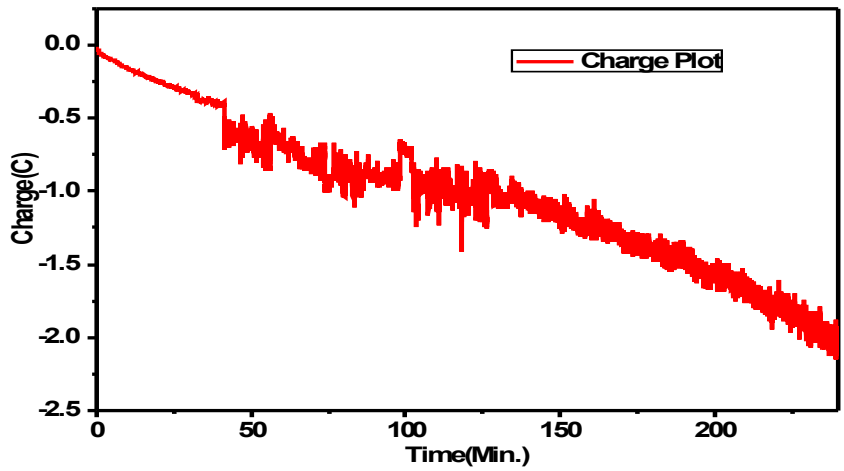

Fig.54 Controlled potential electrolysis Charge plot with CO_2 purging at on potential of 0.6V V/s Ag/AgCl in $NaHCO_3$ +$NaCO_3$ 0.1M Electrolyte

8.6 CuO-$Sr_3Ti_2O_7$

8.6.1 XRD pattern

X-ray diffraction patterns for prepared layered strontium titanate photo catalysts in pure and doped are shown in Fig.55. All the characteristic d-lines for $Sr_3Ti_2O_7$phase are observed in the XRD patterns for neat and doped samples. The amount of dopants being small, no major changes in the XRD patterns for the doped samples are observed

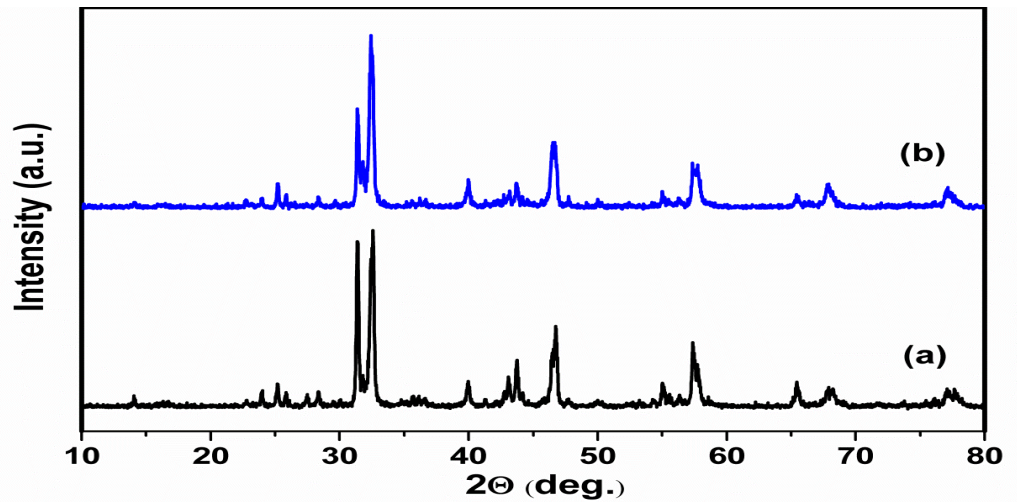

Fig. 55. XRD patterns for neat and doped $Sr_3Ti_2O_7$a. $Sr_3Ti_2O_7$, b. CuO $Sr_3Ti_2O_7$

8.6.2 Linear sweep voltammetry

The figure given below indicates the formation of current is more at initial potential of -2.0V when it was compare with the dark N_2 purging, dark CO_2 purging &Light CO_2 purging. This is due to the formation of more electrons at initial potential of -2.0V.

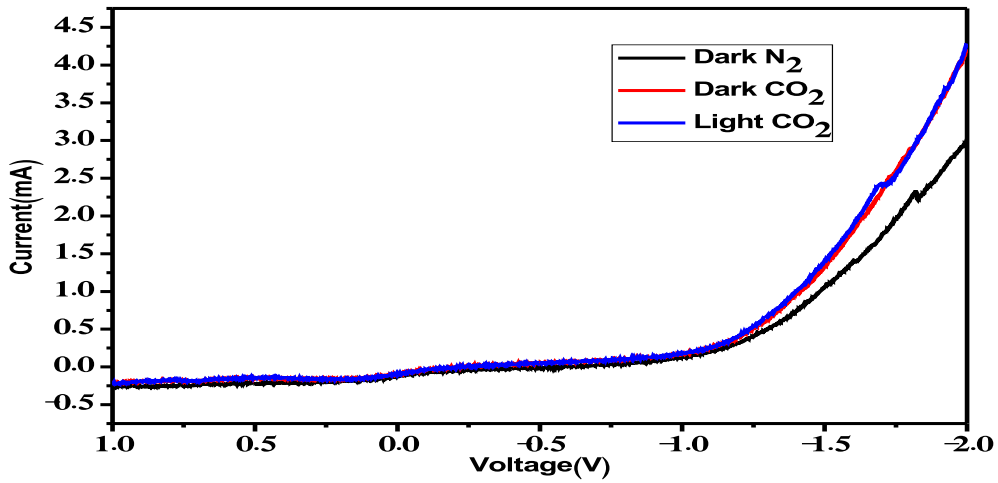

Fig.56 Linear Sweep Voltammetry of $CuO/Sr_3Ti_2O_7$ with and without purging of CO_2 in $NaHCO_3$0.1M Electrolyte at a scan rate of 10mv/s in the presence and absence of light irradiation.

8.6.4 Controlled potential Electrolysis

CPE experiments were performed in three-electrode cell. A Pt foil was used as a counter electrode. The reference electrode was an Ag/AgCl electrode and the working electrode was $CuO/Sr_3Ti_2O_7$. A bias potential of 0.5V V/s Ag/AgCl is applied. The current is increases up to 10 Min. and then stabilizes up to 70 min. Thereafter, the current decreases. Decrease in the charge graph given blow (Fig.57) indicates the formation of hydrocarbon derivates.

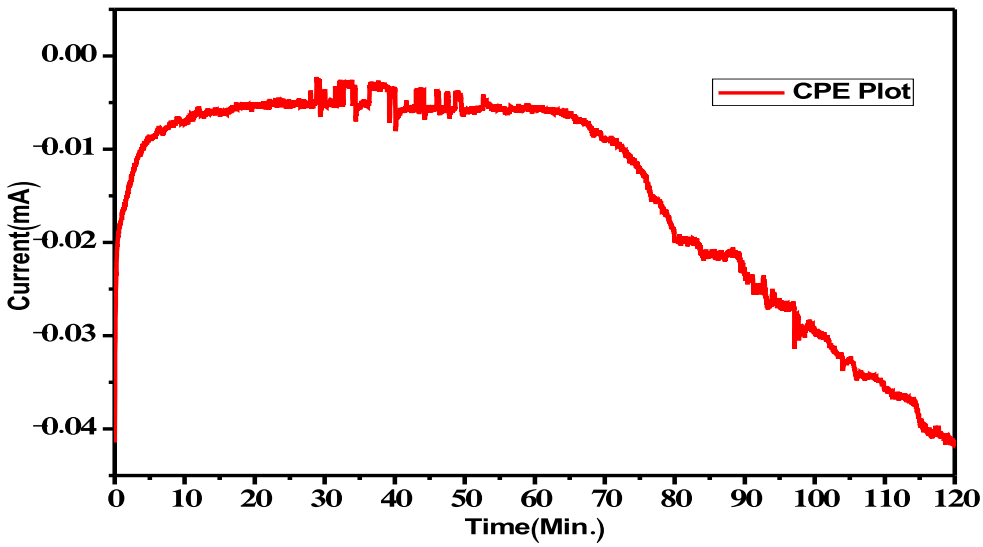

Fig.57 Controlled potential electrolysis with CO_2 purging at on potential of 0.5V V/s Ag/AgCl in $NaHCO_3$0.1M Electrolyte

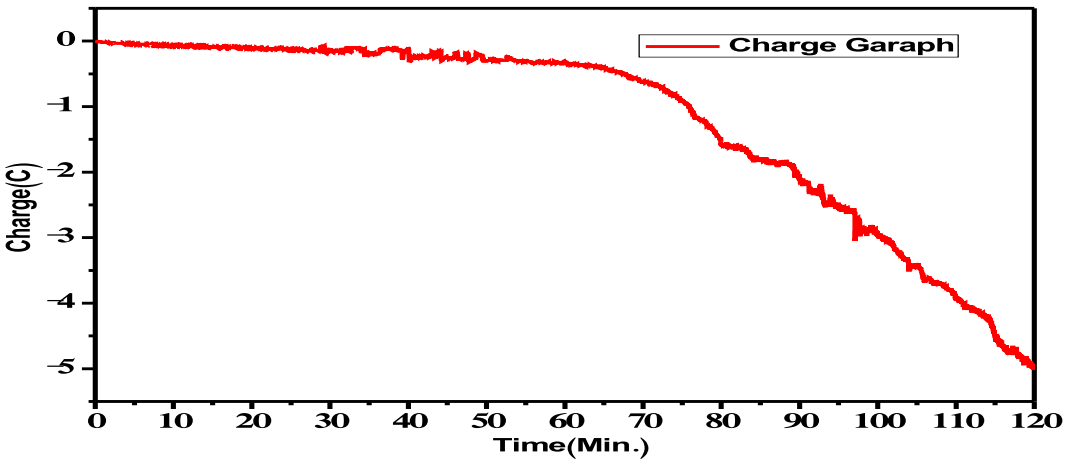

Fig.58 Controlled potential electrolysis Charge graph with CO_2 purging at on potential of 0.5V V/s Ag/AgCl in $NaHCO_3$0.1M Electrolyte

GC analysis of liquid samples from the cathode compartment indicates the presence of trace amounts of methanol and ethanol.

9.STRATEGIES TO IMPROVE HYDROCARBON PRODUCTION BY PECR

9.1. Selection of photo anodes

n-type semi-conductors are used as photo anodes, while p-type semiconductors as photo cathodes. Ideally, n-type semi-conductors are preferred over p-type, since they are stable in presence of electrolytes, without undergoing photo corrosion like n-type. Besides the configuration as shown in Fig.2, with n-type semi-conductors as photo anodes, enables exploring several photo anodes and designing different compensating electrodes/cathode materials so as to maximize the efficiency of the cell

9.2. Increasing electrode area and cell volume

In order to increase the efficiency of PECR of CO_2 attempts were made to increase electrode area Fig. 59 and cell volume (Fig.60)

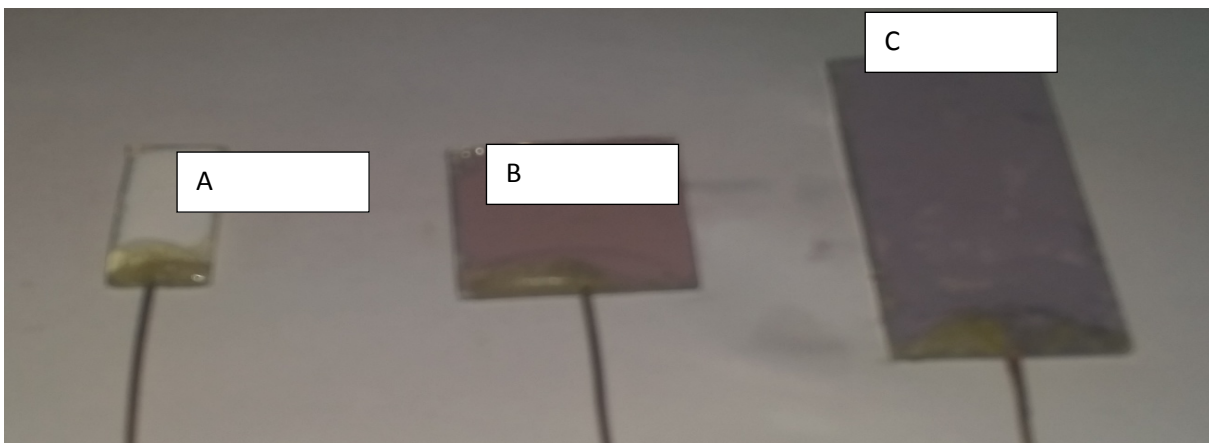

Fig. 59 Photo anodes of different size/ area- A- 3.12 B-6.25 C-12.5 cm^2

In order to have higher quantity of dissolved CO_2 and CO_2 gas volume, the cell volume was increased. Small size cell and large size cells are shown in Fig.60 and Fig.61

Fig.60. Photo electrochemical cell (Small)

Fig.61. Photo electrochemical cell- Large size

9.3. Photo anodes for detailed study

Cyclic voltammetry studies on all the seven catalysts showed reduction of CO_2 at specific applied voltage values. However constant potential electrolysis (CPE) studies indicate that measurable quantities of hydrocarbons due to reduction of CO_2 are formed three catalyst systems, namely,

- Au-N & Fe co-doped $Na_{(1-x)}La_xTaO_{(3+x)}$
- Au-N, S & Fe co-doped $Sr_3Ti_2O_7$
- Au-N, S & Fe co-doped $La_2Ti_2O_7$

Doping with 1%Au was carried out on all the three Fe, N and S modified catalysts, to further improve visible light absorption due to surface plasmon resonance. It is to be noted that all the three catalyst are capable of reducing CO_2 to methane exclusively.

9.4. Strategies to improve PECR of CO_2

For each catalyst, optimum voltage is to be applied in order to get maximum methane formation as shown in Fig.62. Application of voltage > 1.0 V results in the formation of higher carbon number hydrocarbons

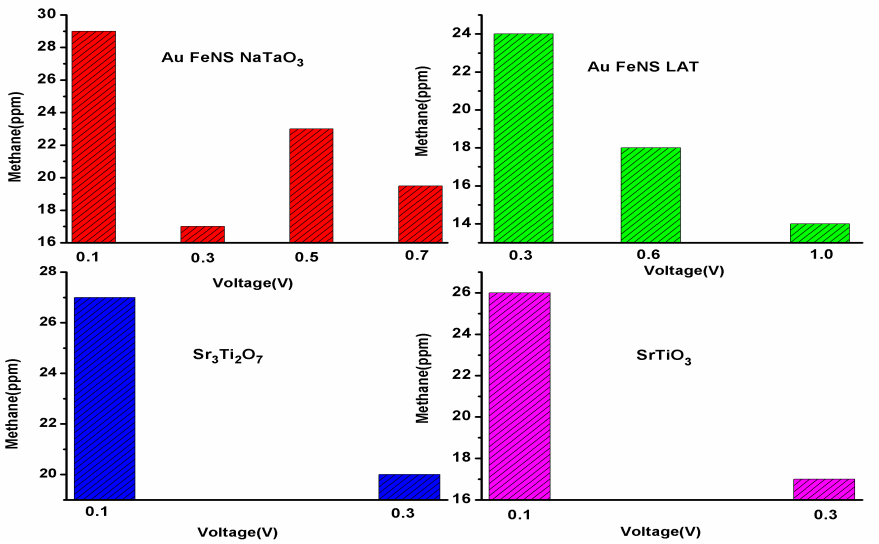

Fig.62. Effect of applied voltage on photo electro cataytic reduction of CO_2 on various photo anodes

Another strategy to improve the efficiency id to increase the phot anode area. Amongst the three photoanode materials investigated, Au-FeNS doped $La_2Ti_2O_7$ displays higher methane production rate of 5.9 nano moles /cm^2 of electrode (cathode) area with a bias voltage of -0.45V, which could be increase to 9.8 nano moles /cm^2 by doubling the electrode area from 6.25 to 12.5 cm^2 as illustrated in Table.2. S and L indicate small and large volume cells designed to accommodate electrodes of small and large areas (Fig.60 & Fig.61, Table 2)

Table.2. Methane formation with different photo anodes- Influence of electrode area and cell volume

Catalysts	Applied from voltage	Methane (ppm)(S)	Rate nmoles/cm² (S)	Rate nmoles/cm² (L)
Au-FeNS-$Sr_3Ti_2O_7$	0.1V	8	2.4	5.2
AuFeNS-$NaTaO_3$	0.1V	11	3.2	7.4
AuFeNS-$La_2Ti_2O_7$	0.45V	20	5.9	9.8

Increasing the electrode area and the volume of the cell/electrolyte are the primary means of increasing hydrocarbon production rate. Doping with Au increases plasmonic absorption of visible light leading to 9.8 nano moles/cm² of methane formation on Au-FeNS-$La_2Ti_2O_7$ in comparison with 6.6 nano moles/cm² realised with the formulation without Au doping.

Table.3. Effect of doping with Au on methane formation

Catalysts	Applied voltage	Methane (ppm)	Rate nmoles/cm² (L)
FeNS-$Sr_3Ti_2O_7$	0.1V	12	5.0
AuFeNS-$Sr_3Ti_2O_7$	0.1V	18	7.4
FeNS-$La_2Ti_2O_7$	0.45V	16	6.6
AuFeNS-$La_2Ti_2O_7$	0.45V	24	9.8

Since the dissolved CO_2 in the aqueous electrolyte solution take part in the reduction process, improving CO_2 solubility is another option to increase production of hydrocarbons. As shown in Table. 4 addition of basic diethanol amine (DEA) to the aqueous $KHCO_3$ electrolyte increases solubility of CO_2 and hence methane formation from 3.2 nano moles/cm² without DEA to 7.1 nano moles/ cm² after adding DEA with Au-FeNS-$NaTaO_3$ as the photo anode and Pt foil as the cathode

Table.4 Effect of addition of organic base on methane formation

Catalysts	Applied voltage	Methane (ppm)	Rate nmoles/cm² (L)

AuFeNS-$NaTaO_3$w/o base	.0.1V	11	3.2
With DEA + CETAB	0.1V	24	7.1

Incorporation of visible light harvesting macro molecules like substituted phenyl porphyrins is another option available to increase visible light absorption. Cu (3,5-dimethoxy) tetra phenyl porphyrin (3,5 Cu-TPP) (Fig.8) in nitrogen doped $SrTiO_3$ increases visible light absorption and accordingly, CO_2 reduction increases (Table 5)

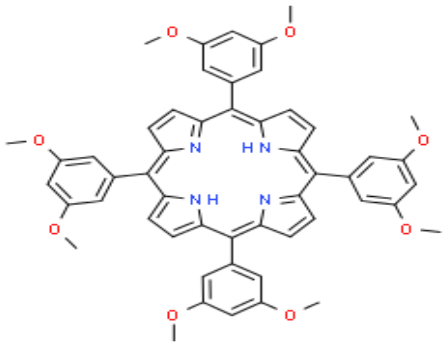

Fig.8. Cu (3,5 methoxy) Tetra Phenyl Porphyrin

Table 5. Influence of sensitization by macro molecules on PECR

Catalysts	Applied voltage (V)	Methane (ppm)	Methanol
N-$SrTiO_3$		18	7
N- $SrTiO_3$ .CuTPP-(3,5 methoxy)	0.1V	22	5

Yet another strategy available to increase CO_2 reduction is to modify the cathode material. As illustrated in Table 6, replacing Pt foil with ITO (Indiun Tin Oxide) plate coated with Pt nano particles increases methane formation from 5.3 to 8.2 nano moles /cm^2. Using copper nano particles deposited on ITO plate as cathode material in the place of Pt foil results in the formation of 35 nano moles/cm^2 of ethylene besides 7.4 nano moles/cm^2 of methane (Table.6).

Using alloy nano particles of Cu & Pt however gives only methane. Thus, by employing several alloy compositions, product selectivity and composition could be varied, while keeping the same photo anode material

Table.6. Influence of different counter electrodes

Working electrode	Counter electrode	Applied voltage (V)	Products n moles/cm2
FeNS-$Sr_3Ti_2O_7$	Pt foil	0.5	5.3 (Methane)
FeNS-$Sr_3Ti_2O_7$	Pt nano	0.5	8.2 (Methane

FeNS-$Sr_3Ti_2O_7$	Cu nano	0.5	7.4 (Methane 35 (Ethylene)
FeNS-$Sr_3Ti_2O_7$	90% Cu-10%Pt nano	0.5	5.7 (Methane

10.SUMMARY AND CONCLUSIONS

The objective of the project was to design different types of working electrodes suitable for photo catalytic reduction of CO_2 to hydrocarbons (PECR). For this purpose H type photo electro catalytic ell with three electrodes, ie., working electrode (WE), reference electrode (Ag/AgCl) (RE) and counter electrode (Pt foil) (CE) fitted with quartz window for irradiation of the WE was designed and fabricated. Experiments were conducted with different electrolytes, $NaHCO_3$, $KHCO_3$ and $NaHCO_3$ + Na_2CO_3 buffer at pH-9.

The other objective is to study the efficiency of semiconductors that are active in the visible region. Accordingly, the following semiconductors with wide band gap have been suitably modified (by doping and sensitization) to reduce the band gap energy and enable visible light absorption and used as working electrode materials.

1. Barium tantalite- $Ba_5Ta_4O_{15}$ modified with N & Fe
2. N,S & Fe co-doped meso porous titania
3. Au-N & Fe modified $Na_{(1-x)}La_xTaO_{(3+x)}$
4. Au-N,S & Fe doped $Sr_3Ti_2O_7$
5. $Sr_3Ti_2O_7$ sensitized with Cu phthalocyanin
6. CuO-$Sr_3Ti_2O_7$
7. Au-N, S & Fe doped $La_2Ti_2O_7$

All the electrode materials have been characterized by XRD, DRS, SEM, EDAX and photo-luminescence spectroscopy. Semi-conductor materials were coated as thin layer on the conducting side of ITO plate and used as working electrodes. With each WE, cyclic voltammetry (CV) and Linear Sweep Voltammetry (LCV) measurements were made to scan specific voltage range and identify the possible CO_2 reduction processes occurring at specified voltages. CPE measurements at these potentials have indicated generation of photo currents and charge transfer. GC analysis of the liquid samples from the cathode compartment has indicated formation of methane as the major reduction product, though traces of ethylene and methanol were observed in some cases.

Amongst the working electrodes studied, Au-Fe-N-S co-doped La-$NaTaO_3$ and Au-Fe-N-S co-doped $Sr_3Ti_2O_7$ and Au-Fe-N-S co-doped $La_2Ti_2O_7$ display stable activity as indicated by

constant current generation and methane formation as indicated by GC analysis. With Au-N, S & Fe co-doped $La_2Ti_2O_7$ as photo anode and Pt foil as counter electrode, 9.8 nano moles /cm^2 of methane formation from CO_2 was observed with the application of very low bias voltage of 0.1 to 0.5 V. Application of higher voltage results in C_2 hydrocarbons

Several strategies have been worked out to improve the hydrocarbon yields.

Increasing the electrode area and the design of electrochemical cell for continuous operation would enhance the potential of this technique for large scale applications. CO_2 from any point source could be used for conversion to hydrocarbons /solar fuels, thus paving way for sustainable energy generation.

REFERENCES

1. **I**nternational Energy Agency CO_2Emissions from Fuel Combustion Highlights **2016.**
2. International Journal of Applied Research 2015; 1(8): 532-533; Michele Aresta. Carbon dioxide as Chemical feedstock, Weinheim, Wiley-VCH Verlag GmbH &Co, 2010, 1-12.
3. M.A. Scibioh, B. Viswanathan, Proc. Indian National Science Academy, 2004, 70A, 407. B. Viswanathan, Materials and processes for solar fuel production, 174, 2014, 211-233.
4. G.Centi and S.Perathoner, ChemSusChem,3 (2010).195-208
5. Z. Jiang, T. Xiao, V. L. Kuznetsov, P. P. Edwards, Phil. Trans. R. Soc. 8 (2010) 3343-3364.
6. T. Inoue, A. Fujishima, K. Honda, Nature, 277 (1979) 637-638.
7. S.C. Roy, O. K. Varghese, M. Paulose, C. A. Grimes, ACS Nano Lett., 4 (2010) 1259-1278.
8. V. P. Indrakanti, J. D. Kubickib,H. H. Schobert , Energy Environ. Sci., 2 (2009) 745–758.
9. V. Jeyalakshmi, R. Mahalakshmi, K.R.Krishnamurthy and B. Viswanathan, Matls.Sci.,Vol.734(2013) p.1-62, TransTech.Pub. Switzerland
10. Y. Izumi, Coord. Chem. Rev. 257 (2013),171.
11. A.Corma and H.Gracia, Journal of Catalysis 308 (2013) 168–175
12. V.Jeyalakshmi, K.R.Krishnamurthy, B.Viswanathan, K.Ramesh, P.V.C.Rao, N.V Choudary and G.SriGanesh, “Catalyst composition for photo catalytic reduction of carbon dioxide” Indian Patent Appl. No.2039/MUM/2013, 17th June,2013

13. M.Gattrel, M.Gupta, A. Co J.Electroanal. Chemistry,594 (2006) 1-19
14. N. S. Spinner, J. A. Vega and W. E. Mustain, Catal. Sci. Technol.,2 (2012) 19–28
15. H. Yano, F. Shirai, M. Nakayama and K. Ogura, J. Electroanal.Chem., 2002, 533, 113.
16. C. M. Sánchez-Sánchez, V. Montiel, D. A. Tryk, A. Aldaz, andA. Fujishima, Pure Appl. Chem., 73(2001) 1917–1927
17. A.Fujishima and K.Honda, Nature (1972) 238,37
18. S.Ichikawa and R.Doi, Catal.Today, (1996) 27, 271-277;Thin solid films,292 (1997) 130-134
19. J. Bockris and J. Wass, J. Electrochem. Soc., 1989, 136, 2521.
20. D. Canfield and K. Frese, J. Electrochem. Soc., 1983, 130, 1772.
21. H. Flaisher, R. Tenne and M. Halmann, J. Electroanal. Chem.,1996, 402, 97.
22. S. Kaneco, H. Katsumata, T. Suzuki and K. Ohta, Chem. Eng. J., 2006, 116, 227.
23. N. Kitamura and S. Tazuke, Chem. Lett., 1983, 12, 1109.
24. J. Lehn and R. Ziessel, Proc. Natl. Acad. Sci. U. S. A., 1982,79, 701.
25. J. Lehn and R. Ziessel, J. Organomet. Chem., 1990, 382, 157.
26. P. Li, H. Wang, J. Xu, H. Jing, J. Zhang, H. Han ,and F. Lu Nanoscale, 2013, 5, 11748–11754
27. Yen-Ping Penga, Yun-Ta Yeha, S. IsmatShahb,c, C.P. Huanga Applied Catalysis B: Environmental 123– 124 (2012) 414– 423
28. C.Genovese, C.Ampelli, S.Perathoner,G.Centi, Journal of Catalysis 308 (2013) 237–249
29. G. Centi, S. Perathoner, G. Winè, M. Gangeri, Green Chem. 9 (2007) 671.
30. S. Perathoner, M. Gangeri, P. Lanzafame, G. Centi, Kinet. Catal.48 (2007) 877.
31. M. Gangeri, S. Perathoner, S. Caudo, G. Centi, J. Amadou, D. Begin, C. Pham-Huu, M.J. Ledoux, J.P. Tessonnier, D.S. Su, R. Schlögl, Catal. Today 143 (2009)
32. C. Genovese, C. Ampelli, S. Perathoner, G. Centi, J. Energy Chem. 22 (2013)202.
33. C. Genovese, C. Ampelli, S. Perathoner, G. Centi, Chem. Eng. Trans. 32 (2013)289.
34. A.S. Bandarenka , M.T.M. Koper, Journal of Catalysis 308 (2013),11-24
35. P. Li, J. Zhang, H.Wang, H. Jing, J. Xu, X. Sui, H. Hu, H. Yin , Catalysis Science & Technology,DOI: 10.1039/C3CY00978E (2014)
36. S. Xie, Q. Zhang, G.Liu and Y.Wang, Chem. Commun., 2016, 52, 35
37. B. Kumar, M. Llorente, J. Froehlich, T. Dang, A. Sathrum and C. P. Kubiak,

Annu. Rev. Phys. Chem., 2012, 63, 541–569.

38. P Wang, S. Wang, H. Wang, Z. Wu, and L. Wang, Part. Part. Syst. Charact. **2018**, 35, 1700371
39. Ning Zhang, Ran Long, Chao Gao* and Yujie Xiong, Sci China Mater 2018, 61(6): 771–805
40. B T-G Xu, C. Zhang, X. Shao, K. Wu, Y-F Zhu, Adv. Funct. Mater., **2006**, 16, 1599–1607.
41. C. C. Li, Y. P. Zheng, T. H. Wang, J. Mater. Chem., 2012, 22, 13216
42. X. Li, J. Zang, J. Phy. Chem. C 2009, 113, 19411.
43. M. Yoshino, M. Kakihana, W.S.Cho, H.Kato, A.Kudo, Chem.Mater. 2002, 14**,** 3369
44. K. S. Lokesh, A. Adriaens, Dyes and Pigments 96 (2013) 269-277
45. C Albay, M Koç, İ. Altın, R. Bayrak, İ. Değirmencioğlu, M. Sökmen, J. Photochem. & Photobiol. A: Chem., 2016, 324, 117
46. Princeton Applied Research, 801 S. Illinois Avenue, Oak Ridge, TN 37830